

Spectropolarimetry of the Type IIb Supernova 2001ig ¹

Justyn R. Maund¹, J. Craig Wheeler¹, Ferdinando Patat², Lifan Wang³, Dietrich Baade²
and Peter A. Höflich⁴

ABSTRACT

We present spectropolarimetric observations of the Type IIb SN 2001ig in NGC 7424; conducted with the ESO VLT FORS1 on 2001 Dec 16, 2002 Jan 3 and 2002 Aug 16 or 13, 31 and 256 days post-explosion. These observations are at three different stages of the SN evolution: (1) The hydrogen-rich photospheric phase, (2) the Type II to Type Ib transitional phase and (3) the nebular phase. At each of these stages, the observations show remarkably different polarization properties as a function of wavelength. We show that the degree of interstellar polarization is 0.17%. The low intrinsic polarization ($\sim 0.2\%$) at the first epoch is consistent with an almost spherical ($< 10\%$ deviation from spherical symmetry) hydrogen dominated ejecta. Similar to SN 1987A and to Type IIP SNe, a sharp increase in the degree of the polarization ($\sim 1\%$) is observed when the outer hydrogen layer becomes optically thin by day 31; only at this epoch is the polarization well described by a “dominant axis.” The polarization angle of the data shows a rotation through $\sim 40^\circ$ between the first and second epochs, indicating that the asymmetries of the first epoch were not directly coupled with those observed at the second epoch. For the most polarized lines, we observe wavelength-dependent loop structures in addition to the dominant axis on the $Q - U$ plane. We show that the polarization properties of Type IIb SNe are roughly similar to one another, but with significant differences arising due to line

¹Department of Astronomy and McDonald Observatory, The University of Texas, 1 University Station C1402, Austin, Texas 78712-0259, U.S.A.; jrm@astro.as.utexas.edu; wheel@astro.as.utexas.edu

²ESO - European Organisation for Astronomical Research in the Southern Hemisphere, Karl-Schwarzschild-Str. 2, 85748 Garching b. München, Germany; fpatat@eso.org; dbaade@eso.org

³Department of Physics, Texas A&M University, College Station, Texas 77843-4242, U.S.A.; wang@physics.tamu.edu

⁴Department of Physics, Florida State University, Tallahassee, Florida 32306-4350, U.S.A.; pah@astro.physics.fsu.edu

blending effects especially with the high velocities observed for SN 2001ig. This suggests that the geometry of SN 2001ig is related to SN 1993J and that these events may have arisen from a similar binary progenitor system.

Subject headings: supernovae: general — supernovae: individual: (SN 2001ig)
— techniques:polarimetric

1. Introduction

Asymmetries are thought to be inherent with core-collapse Supernovae (CCSNe) and are inferred through observations of runaway O stars and pulsars (Dray et al. 2005), spectral line profiles (Mazzali et al. 2005) and, in the extreme, through the link between CCSNe and highly-collimated jets that give rise to Gamma Ray Bursts (GRBs; Woosley & Bloom 2006). Spectropolarimetry has been used to directly measure the geometries of both CC-SNe (Wang et al. 2003b; Leonard et al. 2006) and Type Ia SNe (Wang et al. 2003a). While Mazzali et al. (2005) provide an example of studying asymmetries in CCSNe by examining the shape of line profiles in ordinary spectroscopic observations, spectropolarimetric observations can provide a straightforward and unambiguous measure of asymmetries (Shapiro & Sutherland 1982). The former technique can only be conducted at late times during the nebular phase, when the ejecta is optically thin and the spectrum is dominated by broad emission lines of forbidden transitions. At this later epoch the profiles of these lines can trace the geometry of the ejecta, but are dominated by the Circumstellar Medium (CSM)-ejecta interaction and are no longer necessarily an accurate tracer of the geometry of the explosion mechanism. In addition, during the early, optically-thick phases the profiles of lines are only weakly dependent on the geometry (Howell et al. 2001). Alternatively spectropolarimetry can be conducted at any epoch, especially at early times when the geometry of the ejecta is dictated by the shape of the progenitor and the explosion mechanism. For a spherically-symmetric, electron scattering atmosphere, the polarization vectors of the light received, from different portions of the SN, cancel out leading to no net observed polarization. For geometries that depart from the spherical symmetry, there is incomplete cancellation of the polarization vectors which leads to a net observed linear intrinsic polarization (Shapiro & Sutherland 1982; McCall 1984; McCall et al. 1984). Electron scattering is wavelength independent and the measured level of continuum polarization is associated

¹Based on observations made with ESO Telescopes at the Paranal Observatory, under programmes 68.D-0571 and 69.D-0438.

with the asymmetry of the photosphere. In addition, the polarization associated with spectral lines, through line scattering, yields information concerning the geometry of the line forming region, and specifically the distribution of particular elements within the SN ejecta (Wang et al. 2003b).

SNe are principally classified by the absence (Type I) or presence (Type II) of hydrogen in their early time spectra. All types of SNe except one (Type Ia) are associated with the core-collapse induced explosion at the ends of the lives of massive stars. Wang et al. (2001) showed that, in general, Type II SNe are polarized at much higher levels compared with Type Ia SNe; at $\sim 1\%$ and $\sim 0.2 - 0.3\%$ respectively. Spectropolarimetric studies of the peculiar Type II SN 1987A (Jeffery 1991) and the Type IIP SN 1999em (Wang et al. 2002) showed a significant increase, from 0.1% to 1%, in the level of the polarization as the time since explosion increased, suggesting increasing asymmetries at increasing depths into the SNe. In the case of the Type IIP SN 2004dj (Leonard et al. 2006) the polarization properties were directly correlated to the evolution of the SN light curve. During the optically thick phase, the polarization remained at a nearly constant level; increasing dramatically when the SN entered the optically thin stage, when the complicated internal structure of the core was revealed. Type Ibc SNe demonstrate significantly higher levels of polarization. Spectropolarimetric observations of the Type Ic SN 2002ap showed intrinsic continuum polarization levels $> 1\%$, which Leonard et al. (2002) suggest arises from an asymmetry of at least 20%. In addition, the differences in polarization angles between features due to Fe and other elements demonstrated the different distributions of these elements within the ejecta. Wang et al. (2003b) compared the O I 7774Å line with Fe II lines to show that these elements had very different geometries, and Leonard et al. (2002) similarly studied the difference between Ca lines and those of Fe group elements.

The case of spectropolarimetric observations of Type IIb SNe is particularly interesting, as this type of SN is the link relating H-rich and H-deficient CCSNe. At early times Type IIb SNe show hydrogen in their spectra, but these features weaken over a period of weeks, leading to a hydrogen deficient Type Ib SN (Filippenko, Matheson & Ho 1993; Swartz et al. 1993). The spectroscopic evolution of Type IIb SNe is due to the presence of a thin veil of hydrogen surrounding the core of the progenitor, which is observed at early times but is subsequently dispersed. The principal example of spectropolarimetry of a Type IIb SN comes from observations of SN 1993J. Trammell et al. (1993) and Tran et al. (1997) observed polarizations of $\gtrsim 1\%$, requiring major to minor axis ratios of the emitting region to be between 1.54 and 2. Höflich (1995) modelled these polarizations as being due to asymmetries of the outer H-rich envelope and an off-centre energy source, and Tran et al. (1997) presented the case of an asymmetric circumstellar medium. This is particularly important for the understanding of how the core-collapse mechanism can give rise to a range of SN types. Wang & Wheeler (1996) also showed how, in the case of SN 1987A, the technique of spectropolarimetry may

be used to probe the nature of the dust in the immediate vicinity of SNe at late times. The observations of the Type IIb SN 2001ig and the reduction of the data are given in Section 2. The results of these observations are presented in §3, and are discussed in §4 in the context of SN 2001ig as a CCSN and in the broader context of previous spectropolarimetric observations of other CCSNe, in particular of Type IIb SNe.

2. Observations and Data Reduction

SN 2001ig was discovered by Evans (2001) on 2001 Dec 10.43UT, in the galaxy of NGC 7424. SN 2001ig is located at $\alpha_{2000} = 22^{\text{h}}57^{\text{m}}30^{\text{s}}.7$ and $\delta_{2000} = -41^{\circ}02'26''$ (Ryder et al. 2001), which corresponds to an offset of $185''$ E and $108''$ N from the centre of the host galaxy. The position of SN 2001ig, relative to its host galaxy, is shown as Fig. 1. Ryder et al. (2004) estimated an explosion date of 2001 Dec 3 (JD452247.5), from models of the radio light curve; we adopt this as the reference date for our observations. Phillips et al. (2001) provisionally identified SN 2001ig as being of Type IIb, resembling SN 1987K. Furthermore, Clocchiatti (2002) observed the spectroscopic transition from the H-rich phase to the H-deficient Type Ib phase, confirming the classification of Type IIb. Foreground Galactic reddening, from Schlegel et al. (1998)², is $E(B - V) = 0.01$ or $A_V = 0.03$ assuming a Cardelli et al. (1989) Galactic reddening law. The heliocentric recessional velocity of the host galaxy is given by Koribalski et al. (2004) as 939km s^{-1} . HyperLEDA³ quotes the recessional velocity, corrected for infall towards the Virgo cluster, to be $v_{\text{vir}} = 758\text{km s}^{-1}$; for $H_0 = 75\text{km s}^{-1}$ this corresponds to a distance of 10Mpc.

Spectropolarimetric observations of the Type IIb SN 2001ig were conducted at three epochs: 2001 Dec 16.1, 2002 Jan 3.1 and 2002 Aug 16.3. These observations were made with the Very Large Telescope (VLT) at the European Southern Observatory (ESO), Paranal, Chile; with the Focal Reducer/Low Resolution Spectrograph 1 (FORS1) instrument (Appenzeller et al. 1998). A log of these observations is presented as Table 1. Throughout this study all times are given as UT. At each epoch FORS1 was mounted on Melipal (Unit 3) VLT at the Cassegrain Focus. FORS1, in the spectropolarimetry mode, functions as a dual beam spectropolarimeter. The FORS1 instrument was used with the standard resolution collimator, providing a plate scale of $0.2'' \text{px}^{-1}$. The standard “striped” PMOS slit mask was used, with slit width $1''$ and length $22''$, and for each set of observations the slits were kept at $\text{PA} = 0^\circ$. FORS1 uses a sequence of a “super achromatic” retarder plate and a Wollaston

²<http://nedwww.ipac.caltech.edu>

³<http://leda.univ-lyon1.fr/>

prism (ESO No. 34) to separate the different polarization components. Observations of SN 2001ig were conducted with the retarder plate at 4 angles: 0° , 45° , 22.5° and 67.5° . At each retarder plate position the Wollaston prism produced two beams that were dispersed using the grism G300V, providing a dispersion of 2.6\AA px^{-1} and spectral resolution, measured from arc lamp calibration exposures, of 12.3\AA . The observations covered the wavelength range $4450\text{-}8600\text{\AA}$, when the GG435 order separation filter was used, and $3600\text{-}8600\text{\AA}$, when no filter was used. FORS1 uses a 2048×2048 Tektronix CCD detector, and the observations were conducted with gain $0.71e^- \text{ADU}^{-1}$ and readout noise of $5.6e^-$. The data were reduced in the standard manner using IRAF⁴ and a series of our own routines. The data were corrected for bias and overscan. A master unpolarized normalised flat was constructed from flat observations conducted with the retarder plate at each of the four angles, at each epoch. The flat was applied to object frames, and object spectra, for the ordinary and extraordinary rays at each of the four retarder plate angles, were optimally extracted. These spectra were wavelength calibrated through comparison with observations of HeHgArCd arc lamps. The Stokes parameters Q and U and total polarization p and polarization angle θ were calculated in the standard manner (see Jehin et al. 2005), with the data re-binned to 15\AA to improve the signal-to-noise (S/N) for the individual Stokes parameters. Here we have used a flux binning technique, with bins recalculated prior to the calculation of the Stokes parameters. This yields identical results to the weighted Stokes parameter binning of Wang et al. (1997). The bin size was determined by the spectral resolution of the observations, and was required to be much less than the velocity widths of the SN features (Wang et al. 2003a). A correction was applied for the wavelength dependent chromatic zero angle offset. The total flux spectra of SN 2001ig were flux calibrated using observations of flux standard stars with the retarder plate set to 0° . The data were corrected for the heliocentric recessional velocity of the host galaxy.

3. Observational Results

3.1. Flux Spectra

Flux spectra of SN 2001ig, at the three epochs, are presented as Fig. 2. Velocities at the absorption minima for different lines, in the spectra of 2001 Dec 16 and 2002 Jan 03, are given in Table 2.

⁴IRAF is distributed by the National Optical Astronomy Observatories, which are operated by the Association of Universities for Research in Astronomy, Inc., under cooperative agreement with the National Science Foundation - <http://iraf.noao.edu/>

The spectrum of 2001 Dec 16, at 13 days post-explosion, is dominated by the strong $H\alpha$ P Cygni profile, with an absorption minimum at $-19\,000\text{ km s}^{-1}$. The peculiar profile of the line, with sharp edges separating the emission and absorption components, and a redward shoulder to the emission component suggests blending with He I 6678\AA . This interpretation is further validated by the presence of an absorption “notch” at 6255\AA , corresponding to He I 6678\AA also blue shifted by $-19\,000\text{ km s}^{-1}$. There may also be a contribution to the $H\alpha$ profile due to blended Si II 6355\AA , which is seen in the spectrum of the next epoch’s observation, but this is not resolved at the first epoch. An absorption at 5603\AA is identified as He I 5876\AA ($-14\,000\text{ km s}^{-1}$), however the associated emission feature is not symmetrical about the rest wavelength, the peak is blue ward of the rest wavelength. It may be that the emission feature is truncated by some other feature that lies redward. An absorption feature at the red end of the spectrum is identified as the absorption associated with the Ca II IR triplet ($\sim -12\,700\text{ km s}^{-1}$) - with the emission feature redward of the wavelength limit of the observation. This absorption is, however, blended with a broad telluric feature, as indicated on Fig. 2, increasing the uncertainty on the measured velocity at the true absorption minimum. There is a single absorption at the rest wavelength of Na ID at the recessional velocity of the host galaxy. The measured equivalent width of this feature was determined to be $W_\lambda(\text{NaID}) = 0.7 \pm 0.1\text{\AA}$. Using the relations of Turatto et al. (2003), this equivalent width corresponds to two possible reddenings of $E(B - V) = 0.10$ or 0.32 , which are due to internal reddening in the host galaxy.

The spectrum of 2002 Jan 3, 31 days post-explosion, shows the SN at a transitional state from a Type II to Type Ib SN, with the He lines growing in strength compared to the hydrogen lines. The contamination of $H\alpha$ by lines from other species is more evident. The sharp edge between the absorption and emission components of this profile results from the superposition of Si II 6355\AA , $H\alpha$ and He I 6678\AA . As in the previous epoch, the He I emission component produces a redward shoulder on the $H\alpha$ emission component, and leads to an absorption “notch” at 6415\AA (or $-12\,000\text{ km s}^{-1}$) which suppresses the blue side of the $H\alpha$ emission. The absorption minimum blue ward of the $H\alpha$ peak is characterised by two minima at 6192\AA and 6265\AA , which corresponds to the Si II ($-8\,000\text{ km s}^{-1}$) and $H\alpha$ ($-13\,600\text{ km s}^{-1}$), respectively. He I 5876\AA is observed as a much stronger feature, with obvious emission and absorption components; the absorption minimum corresponds to $-12\,000\text{ km s}^{-1}$. The steep transition blueward from the He I emission to the absorption shows a sharp notch due to Na ID. O I 7774\AA is present as a P Cygni profile with an absorption minimum at 7500\AA , corresponding to $-10\,600\text{ km s}^{-1}$.

The final spectrum, of 2002 Aug 16, 256 days post-explosion, shows the complete transformation of the SN spectrum to the nebular phase, dominated by strong forbidden line emission features, typical of other CCSNe at the nebular phase (e.g. SN 1993J; Matheson et al. 2000b). Most prominent at this epoch is the O I feature at $\lambda\lambda 6300, 6364\text{\AA}$, which shows a

number of peaks that are indicative of asymmetries in the expanding ejecta. A crude Gaussian fit to the O I emission feature gives a full width at half maximum of $6\,700\text{km s}^{-1}$. Also present in the spectrum are features due to Mg I] 4571Å, [Ca II] 7291,7324Å, and emission features due to Fe II 5169Å, HeI 5876Å and O I 7774Å.

3.2. Spectropolarimetric Properties of SN 2001ig

3.2.1. General Spectropolarimetric Properties

The spectropolarimetric observations of SN 2001ig, at the three epochs, are presented as Figs. 3, 4 and 5. The observed polarization properties are a product of both the intrinsic polarization of the SN itself and polarization due to the intervening Interstellar Medium (ISM). The calculation of the latter, the Interstellar Polarization (ISP), is an important consideration and the determination of its quantity is discussed at length in the following sections along with analysis of the intrinsic polarization of the SN. Importantly, the change in the polarization properties between 2001 Dec 16 and 2002 Jan 3 is directly correlated with the evolution in the spectroscopic features in the SN spectrum. The polarization features associated with He I show particularly obvious evolution, with increasing polarization as the He I flux line strength increases at the later epoch. In addition, we note that the observed polarization P.A. in the first epoch varies widely across $\sim 45^\circ$ in the first epoch, whereas in the second epoch the P.A. falls within a narrower range of $\sim 20^\circ$. The polarization features in the second epoch are directly correlated with spectral lines, and for instances with P Cygni profiles we see the classic “inverted P Cygni” profiles in the polarization spectra (Cropper et al. 1988). These profiles are observed for H α , He I 6678Å and O I 7774Å. The observations of the last epoch (2002 Aug 16 or 256 days post-explosion) show that, with the SN having entered the nebular phase, the spectrum is almost completely unpolarized, without significant correlation between polarization features and spectral features. At such late epochs it is presumed that geometric dilution of the scattering particles in the SN ejecta leads to a drop in the scattering optical depth such that, even in the presence of asymmetries, the density of scatterers is not sufficiently high to produce the polarization signature. The amount of scatter in the polarization properties of neighbouring wavelength bins is directly correlated with the S/N and in instances where the S/N is high, as for the $\lambda 4571$ Mg I], $\lambda\lambda 6300, 6334$ Å [O I] lines and $\lambda\lambda 7291, 7324$ [Ca II] lines, the data has small uncertainties and have polarizations tending towards the same values (see §3.2.3).

3.2.2. Data on the Q - U plane

The $Q - U$ plane is a powerful tool for studying the effects of the ISP and simultaneously examining the behaviours of the polarization and the polarization angle with wavelength. This tool has been used to great effect by a number of studies (Cropper et al. 1988; Wang et al. 2003a,b). Wang et al. (2003b) showed how the distribution of the data on the Q - U plane can be parameterised by a “dominant axis,” with functional form:

$$U = \alpha + \beta Q \tag{1}$$

This axis can be used to study and quantify symmetries in the polarization data, which are directly linked to physical axial symmetries in the SN. In addition, Wang et al. (2006) showed that Q and U Stokes parameters across spectral lines have their own “dominant” axes, leading to information about the relative distribution of particular species. Cropper et al. (1988) showed that, for spectropolarimetry of $H\alpha$ of SN 1987A, the progression through the points on the $Q - U$ plane, in wavelength order, yielded a loop structure, as opposed to a simple straight line. This was interpreted as the symmetry axis, of the aspherical SN, having different orientations as a function of wavelength (see also Kasen et al. 2003). The distribution of the spectropolarimetry data of SN 2001ig on the $Q - U$ plane are shown, for each of the three observational epochs, as Figs. 6, 7 and 8.

Since all the observations have been conducted with the slits in the same orientation ($PA = 0^\circ$), all the polarization data presented here has Stokes parameters in the reference frame of the sky. At the first epoch, the concentration of the data on the $Q - U$ plane is obvious, although the location of the dominant axis is not immediately clear. The dominant axis, at each epoch, was calculated using a χ^2_ν minimization technique, that excluded the low S/N red end of the spectrum corresponding to the Ca II IR triplet absorption. The low intrinsic polarization data at the blue end of the spectrum ($< 6000\text{\AA}$) lies on one side of the dominant axis, while the data associated with the $H\alpha$ feature lie on the opposite side of the dominant axis (as shown on Fig. 6). At the second epoch the dominant axis is clearly defined and has rotated through $\sim 40^\circ$ compared to the first epoch. The data is more tightly clustered on the $Q - U$ plane, which is partially due to an improvement in the S/N at the second epoch as the SN had just reached maximum by day 31. The difference in the locus of the data, on the $Q - U$ plane, at the two different epochs results in two different values of β (even after ISP subtraction, as discussed in Section 3.2.3). The data at day 256 show no discernible structure and are dominated by the statistical uncertainty due to the faintness of the SN, compared to earlier epochs, and, hence, low S/N. The use of a dominant axis to describe the data at the third epoch was, therefore, inappropriate.

The dominant axis defines a useful “zero point” for rotating the Stokes Parameters to a more meaningful reference frame than that defined by using $PA = 0^\circ$ on the sky. The Q and

U parameters can be rotated using the standard two-dimensional rotation transformation, given by (Wang et al. 2003a) as:

$$P_d = (Q - Q_{ISP}) \cos 2\theta_d + (U - U_{ISP}) \sin 2\theta_d \quad (2)$$

$$P_o = -(Q - Q_{ISP}) \sin 2\theta_d + (U - U_{ISP}) \cos 2\theta_d \quad (3)$$

where θ_d is the polarization angle of the dominant axis, determined from Eqn. 1, and the P_o is the polarization in the orthogonal direction on the $Q - U$ plane but corresponds to a physical rotation of 45° . To ensure rotation about an origin of zero intrinsic polarization of the SN, the rotated Stokes parameters are calculated using the Stokes parameters corrected for the ISP (see §3.2.3). The rotated Stokes parameters for the data of 2001 Dec 16 and 2002 Jan 03 are shown as Figs. 9 and 10, respectively.

3.2.3. Determination of the Interstellar Polarization

The correct study of the intrinsic polarization properties of SN 2001ig requires careful accounting for and subtraction of polarization due to the intervening ISM. Serkowski et al. (1975) present the relationship between reddening and the ISP, where $p_{ISP}(\%) < 9E(B - V)$ for Galactic type reddening and dust polarization laws. This relationship can be used to place important maximum limits of the total B/V polarization using reddenings determined from non-polarimetric techniques. We assume that dust in the host galaxy NGC 7424 follows similar reddening and polarization laws as the Galaxy, although studies by Leonard et al. (2002) and Clayton et al. (2004) suggest that this may not be the case. The maximum polarization due to the Galactic ISM is 0.09%, given $E(B - V) = 0.01$. In addition, the reddening calculated from the equivalent width of the Na ID lines, in §3.1, yields two limits on the polarization, due to the ISM of the host galaxy, as 0.9% and 2.9%. Under the assumption that the Galactic polarization law holds in NGC 7424, these are strict upper limits on the ISP (including the relevant uncertainties in the measurements of the equivalent width and in the calculation of the reddening). These limits describe a circle on the $Q - U$ plane, and comparison of Figs. 6 to 8 shows that the observed data have polarizations significantly lower than these limits.

Trammell et al. (1993) and Tran et al. (1997) assume that the P Cygni emission components of lines such as $H\alpha$ are inherently depolarized, such that any residual polarization across the emission features is due solely to the ISP. At the first epoch, Figs. 3 and 6, the $H\alpha$ emission component has one of the highest polarization levels across the observed wavelengths. The $H\alpha$ profile, as discussed in Section 3.1, is a product of both $H\alpha$ emission and the blueward absorption associated with the He I 6678Å. In this case, therefore, the polarization observed across $H\alpha$ is obviously not the ideal case of a completely depolarized emission component of

one line and, hence, precludes the use of this assumption for determining the ISP.

As we have observations at more than one epoch, it is possible to calculate the ISP as a non-varying quantity, with a single polarization angle, by comparing the behaviour of SN 2001ig on the $Q-U$ plane at different epochs. There could also be a local, variable, polarized source within the seeing disk of these observations; there is no known technique to correct for such phenomena. As noted in §3.2.1, the data show a large rotation and an increase in polarization between the first and second epochs, corresponding to the change from an H-rich spectrum to a transitional He-rich spectrum. The ISP is, by assumption, constant between the two epochs, requiring our choice of ISP to be applicable to both cases. Furthermore, following Howell et al. (2001) and Wang et al. (2003a), we expect the ISP to be located at one end of the dominant axis of the locus of the data on the $Q-U$ plane and in the proximity of the data at bluer wavelengths, due to high degree of blending and, hence, depolarization of Fe II lines at bluer wavelengths. For the data of the first epoch (Fig. 6) we note that the Q and U of the lowest total polarization features limit the ISP to $Q_{ISP} < 0.2$, $U_{ISP} > -0.2$. For the second epoch, shown as Fig. 7, the dominant axis is easily identified, and the ISP must be located at the low polarization end of the distribution of data along the dominant axis (since an ISP located at the opposite high-polarization end of the data distribution would be inconsistent with the observed data of the first epoch). The data of the second epoch limits the ISP Stokes parameters to $Q_{ISP} < 0.3\%$ and $U_{ISP} < 0.1\%$.

The observation at the third epoch shows the SN in the nebular phase, when the density of scattering particles is extremely low. At this epoch it is expected that the density is insufficient to produce a net intrinsic polarization, rather that the observed polarization at this epoch is just due to the combined ISP of the foreground and host galaxy ISP. The average values of Q and U data would therefore be equivalent to Q_{ISP} and U_{ISP} . In order to use this data to determine an ISP, the data were rebinned to 50\AA to improve the S/N. The polarization signature at the red end of the data suffers from low S/N, due to the response function of FORS1 at those wavelengths. This leads to a polarization signature with larger uncertainties. This section of the spectrum, with $\lambda > 8000\text{\AA}$, was removed from the calculation. The rebinning of the spectrum, and removal of high-uncertainty wavelength range, significantly reduced the scatter in the data and the centroid of the data on the $Q-U$ plane was measured, using separate weighted averages for both Q and U , to be $\overline{Q} = 0.12 \pm 0.07$ and $\overline{U} = -0.12 \pm 0.08$. The quoted uncertainties on these values are the standard deviations, which provide a better estimate of the scatter than the standard error on the mean. These values are consistent with the limits placed on them using the observations from the first and second epochs, and are the same as the measured Stokes parameters in the regions of the spectrum of the third epoch with the highest S/N (see §3.2.1).

The Serkowski et al. (1975) form of the ISP has only a small degree of λ -dependence, across the wavelength range being studied here. The small value of the determined Stokes pa-

rameters of the ISP are sufficiently low that any effects due to the λ -dependence of the ISP would be much less than the quoted uncertainties. We adopt, therefore, values of the ISP Stokes parameters of $Q_{ISP} = 0.12 \pm 0.07$ and $U_{ISP} = -0.12 \pm 0.08$, corresponding to $p_{ISP} = 0.17 \pm 0.08$ and $\theta_{ISP} = 157.5^\circ$ (which is in the direction tangential to the host spiral arm in NGC 7424, as shown on Fig. 1; Scarrott et al. 1987). These values limit the reddening, assuming a Galactic polarization law, to $E(B - V) > 0.01$ as a lower limit, requiring a reddening component in addition to the Galactic foreground reddening.

Correction of the ISP requires the vectorial subtraction of Q and U , effectively an offset of the zero-point of the intrinsic Q and U parameters from the observed Stokes parameters. The principal ramification of this property is that the corrected total polarization $p_0 \neq p_{obs} - p_{ISP}$, and polarized features can become depolarized and vice versa. The polarization spectra, after correction for the ISP, are also shown for the three observational epochs as Figs. 3, 4 and 5.

Howell et al. (2001) suggest that the region between 4800-5600Å should be depolarizing, since in that wavelength range the line blanketing opacity of Fe II lines dominates over electron scattering, leading to net depolarization. We note that in the case of SN 2001ig, however, the observed polarization over much of that wavelength range is similar in magnitude to that observed for H α for which the presence of net intrinsic polarization has already been discussed. The narrower wavelength region of 4600-4800Å shows lower levels of polarization, at the first epoch, than 4800-5600Å. Only in the narrower region 4600-4800Å is there almost complete depolarization evident, with the observed polarization consistent with the ISP alone (see Fig. 6). The Fe II lines are further discussed in §3.2.6.

3.2.4. H α , Si II and He I 6678Å

At the first epoch, the H α polarization signature seems counter-intuitive, with the maximum polarization of this feature observed at 6350Å, near the emission peak in the flux spectrum, and minimum polarization reached just blueward of the absorption minimum. Low polarization is generally seen for the entire absorption feature (see Fig. 3), with the Stokes parameters lying on or close to the dominant axis with no obvious loop structure (Figs. 9 and 11a). At day 31, the blue edge of the H α /Si II absorption profile (~ 6100 Å) is coincident with a peak in polarization of 0.7% (Figs. 4 and 10). Significant polarization is observed at both of the flux minima of H α and Si II, but it is smaller in magnitude than the polarization at the blue edge. Redward of the flux absorption minima is a partly depolarized region at 6300Å associated with the H α emission. The polarization has a local minimum of 0.2% at the location of the He I 6678Å emission component. Within this depolarized

wavelength range there is, however, a peak in polarization at $\sim 6400\text{\AA}$, comparable to that observed for the blue edge of the $\text{H}\alpha/\text{Si II}$ absorption profile. This peak coincides with the absorption minimum of the He I 6678\AA P Cygni profile, the prominent “notch” at 6400\AA in the flux spectrum (Figs. 4 and 10). This polarization signature across the He I 6678\AA absorption minimum matches the polarization peak observed for the absorption minimum of He I 5876\AA , where the peak polarizations are equal and the Stokes Parameters are observed to rotate through 10° .

The behaviour of the blended $\text{H}\alpha/\text{He I}/\text{Si II}$ feature on the Q-U plane, presented in Fig. 12a, shows that data at these wavelengths are aligned with the dominant axis, but that the H I absorption feature forms a loop deviating from a straight line by $\pm 0.2\%$, in the direction orthogonal to the dominant axis. The rotated Stokes parameters at this epoch (Fig. 10) actually resolve the separate structures of the blend. A peak in the orthogonal rotated Stokes parameter is associated with the absorption minimum of $\text{H}\alpha$ in the flux spectrum, but there is no corresponding feature in P_d . The absorption feature associated with He I 6678\AA giving rise to the “notch” in the blended profile in the flux spectrum, is, conversely, only observed in P_d and not in P_o . The loop structure observed on the $Q - U$ plane for this blend is, therefore, due to the superposition of two lines arising from different species with different geometries within the ejecta. By day 256, $\text{H}\alpha$ nebular emission is not significantly detected in the flux spectrum and there is no significant polarization at the expected wavelength for this line.

3.2.5. O I 7774\AA

The O I 7774\AA feature is observed in the flux spectra at all epochs, and in the case of the last epoch it is only seen in emission. At the first epoch there is no excess polarization, over the wavelength range of the O I 7774\AA line (which is observed at the second epoch) as shown in Fig. 11b. At 2002 Jan 3, the standard polarization profile expected for P Cygni spectroscopic profiles is observed, with peak polarization (0.7%) associated with the absorption component at $\sim 7500\text{\AA}$ and decreasing levels of polarization to a minimum of 0.3% at the peak of the emission component (Fig. 4). These maxima and minima are similar to the observed polarization levels of $\text{H}\alpha$ and He I 6678\AA . The presence of a telluric absorption band at the wavelengths of this feature complicates both the spectroscopic and spectropolarimetric interpretation of this line. There is sufficient resolution, even with the data rebinned, to safely identify those bins with high uncertainties on the Stokes parameters and exclude them from the analysis. On the $Q - U$ plane, on Fig. 12b, the O I data points are tightly clustered about the dominant axis, with a maximum deviation in the orthogonal direction of $\pm 0.17\%$. The O I 7774\AA is almost completely described by P_d , with nearly no

signal or variability in P_o over the entire line profile (Fig. 10). At day 256, 2002 Aug 16, the line is observed in emission, and there is no significant polarization signature associated with it.

3.2.6. *Fe II*

The wavelength range from 4800-5400Å is expected to be mostly composed of Fe II lines, with their overlap (due to Doppler broadening) leading to depolarization across this wavelength range (Howell et al. 2001). At day 13, there is a net polarization of 0.2% observed across this range. This is likely due to the presence of strong polarization signatures from other lines, due to other species, which cannot be completely depolarized by the Fe II lines; for example, Fe II 4924Å blended with H β and He 4921Å, and 5018Å blended with He 5015Å (Matheson et al. 2000a). The Stokes parameters show no preferred orientation across the Fe II lines (Figs. 9 and 11c) and a rise in the dominant rotated Stokes parameter across the wavelength range is interpreted as being due to blending with other species. At day 31, a net depolarization from 0.5% to 0.1%, compared to other features, is observed across this wavelength range. The effects of possible blending are illustrated by the proximity of H β , blueward, and He I 5876Å redward. Taking the wavelength range of 4800-5400Å as being representative of a number of Fe II lines, the data on the $Q - U$ plane and the dominant and orthogonal rotated Stokes parameters shows that the associated polarization is well described by the dominant axis (see Figs. 10 and 12c) with minor deviations due to the behaviour specific to individual lines of either Fe II or blends of Fe II lines with those other species (Matheson et al. 2000a). The cause of the polarization peak at the second epoch at 4750Å is unclear, given the high density of Fe II lines and H β . The polarization feature is significantly broader than any of the individual absorption features, in that wavelength range, observed in the flux spectrum. This implies that it is unlikely that a single line is producing it. This polarization is only observed along the dominant axis (Fig. 10 and 12c), unlike H α . It is, therefore, unlikely to be due solely to H β and since it would be expected to have similar polarization properties as H α . It is more likely to have arisen from Fe II lines as it is oriented along the dominant axis, similar to the polarization properties measured for the Fe II lines at larger wavelengths.

3.2.7. *Ca II IR triplet*

The polarization properties of the Ca II IR triplet absorption feature suffer from a number of effects which increase the levels of uncertainties on the measurements. The region

redward of 8000\AA shows a significant drop in the response of the FORS1 detector and hosts a particularly broad telluric absorption band. At the first epoch, there is a polarization associated with the absorption feature, that reaches a maximum degree of polarization of $0.4 \pm 0.3\%$ at the absorption minimum (see Fig. 11d). At day 31, with increased S/N in the red, due to the increased brightness of the SN, the maximum polarization is again observed to directly correlate with the absorption minimum and is measured as $0.7 \pm 0.2\%$. As for the O I 7774\AA line, the uncertainties of the measured Stokes parameters are large and this is due to the telluric absorption band. At the red extreme, the profile of the Ca II IR blended triplet absorption, in the flux spectrum, appears rising towards the emission component. The polarization angle is observed to rotate from the continuum polarization angle of $\sim 40^\circ$ through $+20^\circ$ moving redward towards the absorption minimum and back through -20° when moving from the absorption minimum toward the unobserved emission component. On the $Q-U$ plane, see Fig. 12d, an incomplete loop is observed, as the emission component was not observed. The loop appears to be aligned with the direction orthogonal to the dominant axis (deviating by a maximum 0.4%), and is approximately parallel to the dominant axis determined for the observations of day 13. The rotated Stokes parameters P_d and P_o show that at day 13 the polarization of the Ca II is parallel to the dominant axis (Fig. 9). By day 31, however, the polarization has substantial components in both P_d and P_o (Fig. 10). At day 256, there is no significant polarization associated with the Ca II IR triplet, with large error bars being symptomatic of the low S/N at these wavelengths.

4. Discussion

The observations of SN 2001ig show the three distinct epochs in the spectroscopic evolution of a Type IIb SN, accompanied with three distinct sets of polarization properties. The flux spectra of SN 2001ig at all three epochs are compared on Fig. 2 with spectroscopic observations of SN 1993J, obtained from the SUSPECT archive⁵. At the earliest epoch, SN 2001ig is observed to have a higher ratio of Balmer to helium line strengths than SN 1993J. Indeed, at this epoch the spectrum of SN 2001ig is more similar to that of SN 1987K (Filippenko 1988; Clochiatti 2002), with the absorption of He I 6678\AA at higher velocities and, therefore, being observed to be blueward of $H\alpha$. The absorption minimum of $H\alpha$ however, is observed to be significantly more blueshifted, by $\sim 3500\text{km s}^{-1}$, than observed for 1987K. Similarly, at 31 days the absorption of He I 6678\AA is at higher velocities than was observed for SN 1993J at a similar epoch (12000 vs. 6940km s^{-1} ; Swartz et al. 1993). In the nebular phase, at day 256, the spectrum of SN 2001ig is very similar to SN 1993J at

⁵<http://bruford.nhn.ou.edu/~suspect/>

a similar age showing [Ca II] 7291,7324Å, He I 5876Å and O I 6300/6364Å. The ratios of the strengths of these lines in SN 2001ig are approximately similar to those observed for SN 1987K and SN 1993J (Filippenko 1988; Matheson et al. 2000a; Ryder et al. 2006), although Filippenko & Chornock (2002) note that the Mg I] 4471Å observed for SN 2001ig is particularly strong (see Fig. 2).

At 13 days, when hydrogen features dominate the spectrum, the general spectrum-wide polarization is low $\sim 0.2\%$. This is consistent with the low polarizations observed for Type IIP SNe (Wang et al. 2002; Leonard et al. 2001) which have extended optically-thick hydrogen envelopes. The presence of a non-zero polarization implies that there is an asymmetry of the outer hydrogen layers at the early times; which for an edge-on oblate spheroidal configuration only requires an axis ratio of ~ 0.9 (Höfllich 1991).

It is only at the second epoch when the expected depolarized H α emission feature is first observed. This is due to the decrease in the velocities of the ejecta material compared to the first epoch, which changes the way in which the absorption and emission features of H α and He I 6678Å are blended. The increase in polarization of SN 2001ig between the first and second epochs is also similar to other Type II SNe, when the hydrogen layers cease to be optically thick and the interior asymmetric He core is revealed (e.g. SN 1987A, Jeffery 1991; SN 2004dj, Leonard et al. 2006).

The evolution in the polarization signature of SN 2001ig at the first and second epochs is matched by the spectroscopic evolution of the SN, with the increase in the strength of helium lines by the second epoch. The data on the $Q - U$ plane, at this epoch, are aligned with an obvious dominant axis which suggests that the He core layer asymmetries still retain a strong axial symmetry although clearly not a spherical symmetry (Wang et al. 2003b). The dominant axis determined for the data at the second epoch is, however, almost orthogonal to the dominant axis of the data at the first epoch. This suggests that while asymmetries were present at day 13, they were not coupled to the larger asymmetries present in the core that were revealed by day 31 in either the degree of the asymmetry or the orientation of the asymmetry on the sky. This provides a case, therefore, that the hydrogen envelope was sufficiently extended to not be directly coupled to the asymmetries of the He core layers due to the explosion mechanism. Höfllich (1995) suggested that the small degree of early polarization observed for SN 1993J was due to tidal distortion of the progenitor by a binary companion, if the SN arose in such a system. Alternatively, or in addition, another source of polarization at the earlier epoch might be the aspherical distribution of sources of excitation, from newly synthesized material, causing the shape of the photosphere to deviate from a spherical symmetry, while the density distribution of the hydrogen envelope remains physically spherically symmetric (Höfllich et al. 2001). The asymmetry measured at the first epoch is, perhaps, an upper limit on the physical asymmetry of the hydrogen envelope.

SN 2001ig and SN 1993J exhibit the same evolution in polarization properties between days

13 and 31, with an increase in the degree of the polarization accompanied by the rotation of the polarization axis. At the first epoch, the V -band polarization of SN 2001ig (from synthetic broad-band polarimetry) is 0.3% with $\theta = 185^\circ$ (ISP subtracted), whereas SN 1993J was polarized at a level of $\sim 0.6\%$ at approximately the same epoch (1993 Apr 7; Tran et al. 1997). At 31 days, the broad-band V polarization for SN 2001ig is 0.6%, whereas the polarization of SN 1993J was 0.8% (1993 Apr 26; Tran et al. 1997), and the polarization angle had rotated through $\sim 40^\circ$. In absorption components, however, SN 2001ig is less polarized than SN 1993J by $\lesssim 1\%$. The meandering path of the V -band polarization of SN 1993J, as plotted on the $Q - U$ plane (see Fig. 10 of Tran et al. 1997), is also seen for SN 2001ig; although the number of observational epochs of SN 2001ig is much lower.

In these respects SN 2001ig is similar to 1993J, but there are important exceptions. At day 31 the polarizations of the He I 5876Å and 6678Å absorption minima of SN 2001ig are comparable to that of the $H\alpha$ absorption feature, whereas there is no observed polarization signature attributable to He 6678Å in SN 1993J. This is due to the He I 6678Å line for SN 2001ig being both stronger and having a higher velocity than was observed for the same line in SN 1993J. The higher velocity for the absorption of He I 6678Å means that it is not completely coincident with the depolarizing $H\alpha$ emission flux, such that the polarization signature of the absorption is still observed.

Wang et al. (2001) suggested that the classification of a CCSN as being of Type IIb might depend on the orientation of the SN as seen by the observer, given the spectropolarimetric similarity between SN 1993J and SN 1996cb. The observations presented here have shown that SN 2001ig arises from the same family of SNe as SN 1993J and SN 1996cb and, by extension due to spectroscopic similarity, to SN 1987K, but that Type IIb SNe are not as homogeneous as suggested by Wang et al. (2001). In the context of Type I CCSNe, we note that a whole range of polarizations have been measured for Type Ib/c SNe, from $\sim 1\%$ for SN 2002ap (Mazzali et al. 2005; Wang et al. 2003b; Leonard et al. 2002) to $\gtrsim 4\%$ for the Type Ic SN 1997X (although this is a broad band polarization measurement and it is unclear if this value is representative of the continuum polarization; Wang et al. 2001). On the other hand Type IIP and IIb SNe exhibit a more limited range in polarization than the more hydrogen deficient SNe. This suggests that the retained hydrogen envelope of the progenitor is important to dictating the polarization evolution of Type IIb SNe, and that Type IIb SNe which have undergone the transition to the hydrogen poor phase are not necessarily the same as “pure” Type Ib SNe.

Particular note is made of the loop structure observed, on the $Q - U$ plane, for certain spectral lines. Loops were observed in spectropolarimetry of SN 1987A (Cropper et al. 1988) and similarly have been presented for the Type Ia SN 2001el (Kasen et al. 2003). The production of a loop requires an increase (or a decrease) in polarization across a spectral line, accompanied by a rotation in polarization angle. While Wang et al. (2003b) discussed the

“dominant” and “orthogonal” axes, a loop is a mixture of both. The rotated Stokes parameters of the Ca II IR triplet cannot be decomposed at day 31 to two distinct orthogonal components (Fig. 10), leading to loop structure on the $Q-U$ plane (Fig. 12a). The H α /He I blend is not, however, a true loop since it can be decomposed into two orthogonal components depending on which element dominates absorption at a particular wavelength. Kasen et al. (2003) discussed how loops may be formed by breaking a global axial symmetry by having varying degrees of the departure of the ejecta from an axial symmetry as a function of depth or with a clumpy SN ejecta. The loops may hint at the presence of plume-like structure in SN 2001ig ejecta, which is observed in SN remnants (Fesen & Gundersen 1996).

Wang et al. (2006) applied straight line fits to the Stokes parameters on the $Q-U$ plane to judge the relative distributions of particular elements within the ejecta of the Type Ia SN 2004dt. If spectral lines produce loops rather than a single dominant axis (i.e. a straight line) on the $Q-U$ plane, then straight-line fits of a dominant axis to a loop would be inappropriate; this may then explain the high values of χ^2_ν that Wang et al. found for fitting dominant axes to a number of spectral features of SN 2004dt.

The locations of loops, hence the range of polarization angles, on the $Q-U$ plane can be used in a similar manner to fits of the dominant axes to particular spectral features to look for the relative distributions of different elements within the SN ejecta. For day 31, species such as He and O are observed to have similar orientations on the $Q-U$ plane and all lie along the dominant axis (see Figs. 10 and 12c), suggesting a similar distribution for these elements in the ejecta. The polarization of H α , however, is predominantly orthogonal to these species and, hence, has a significantly different distribution within the ejecta. The Stokes parameters across the Ca II absorption feature, however, seem to have a similar orientation to the dominant axis measured for day 13.

The nature of the progenitor system, single or binary, that gave rise to SN 2001ig has been subject to much debate. Ryder et al. (2004) observed periodic fluctuations in the radio light curve of SN 2001ig, due to fluctuations in the CSM density. Ryder et al. concluded that this was due to the presence of a binary companion, disturbing the stellar wind from the progenitor as the immediate CSM was formed, with the periodicity in the density fluctuations corresponding to the orbit of the companion. Kotak & Vink (2006) suggested, however, that episodic mass loss from a Luminous Blue Variable phase of the progenitor could also produce similar density fluctuations in the CSM. Additionally Soderberg et al. (2006) showed that SN 2003bg had a similar radio light curve to SN 2001ig; the likelihood of two systems having the same orientation and binary progenitor system parameters, to produce such similar light curves, was considered to be too low to make a binary progenitor a plausible scenario based on radio measurements alone. In the case of the Type IIb SN 1993J, the progenitor was identified in fortuitous pre-explosion images (Aldering et al. 1994) and the companion was identified in very late time images and spectroscopy (Maund et al. 2004), demonstrating the

production of that particular Type IIb SN from a binary progenitor system. Ryder et al. (2006) have claimed to observe a possible stellar source, 3 years post-explosion, at the site of the fading remnant of SN 2001ig. It is, therefore, particularly interesting to discuss the observations presented here in the context of the nature of the progenitor system. Wang et al. (2001) concluded that Type IIb SNe, having so many similar spectropolarimetric properties, must arise with similar orientations to the observer. The shared characteristics of SN 2001ig with Type IIb SNe 1993J and 1996cb, while not a complete match, might suggest a common type of progenitor with similar orientation; thus favouring a binary progenitor. The differences in the polarization properties observed for SN 2001ig days 13 and 31 suggests that the hydrogen and core layers did not possess the same asymmetry, both in degree and orientation. The hydrogen envelope was, therefore, sufficiently large (in radius) to not be subject to the same asymmetries as the core; this is in contrast to the picture of Soderberg et al. (2006), who suggest a thin hydrogen layer on a Wolf-Rayet progenitor.

In both the jet-torus model (Höfllich et al. 2001) and the binary progenitor system model (Höfllich 1995), it is clear how different asymmetries of the envelope and the core-layers (defined by the physically orthogonal equatorial plane and rotational axis of the progenitor) would lead to different polarization angles for the dominant axis between the first two epochs. In the jet-torus model, the production of Ni in a jet would cause asymmetric excitation of the hydrogen envelope aligned with the rotational axis, while the core-layers would form a torus in the equatorial plane. In the binary progenitor model, the asymmetries of the hydrogen envelope would be caused by tidal interaction with the companion, causing deformation in the direction of the equatorial/orbital plane, and a jet, that did not breach the outer core-layers, would cause elongation of the core-layers along the rotational axis. Neither of these two simple models can explain the physical rotation of the asymmetries, between the first and second epochs, of only $\sim 40^\circ$ when both favor a rotation of 90° .

Alternatively, Maund et al. (2007) present a "tilted jet" model. In this model the jet axis is not aligned with the rotational axis of the progenitor, such that the outer layers and the inner core layers do not have to have either the same or orthogonal axes of symmetry. The outer layers, in this model, retain the shape of the progenitor, but the core-layers are elongated by the mechanical force of the jet and the redistribution of Ni along the jet axis. In the tilted-jet model, the angle between the axis of symmetry of the core and the outer layers is not fixed. We note that the polarization axis of SN 1987A is tilted by $\sim 15^\circ$ with respect to that of the circumstellar rings (Wang et al. 2002) and similar deviations might characterize Cas A (Wheeler et al. 2007). The Standing Accretion Shock Instability in 3-D may provide a mechanism through which the axis at which the jet is launched is no longer aligned with the rotational axis of the progenitor, with Blondin & Mezzacappa (2007) modelling the rotational axis of the proto-neutron star, in 3-D core-collapse simulations, becoming misaligned by angles such as 10° , 15° and 45° from the rotational axis of the Fe core. Other

non-axisymmetric instabilities may also play a role (Wheeler & Akiyama 2007).

It is clear, however, that along with appropriate models spectropolarimetry data can provide important insight into the nature of the explosion mechanism and the progenitors of this type of CCSNe.

5. Conclusions

The Type IIb SN 2001ig has been observed to have a strong polarization signature, consistent with other Type IIb SNe. The polarization properties are generally in excess of those observed for Type IIP SNe, but at the lower limit of polarizations observed for the hydrogen deficient Type Ibc SNe. The ISP is constrained by analyzing the polarization behaviour of SN 2001ig at three separate epochs, but particularly using observations at the last epoch, in the nebular phase, when SN 2001ig is believed to be intrinsically unpolarized. SN 2001ig has a low continuum polarization of 0.3% at 13 days, consistent with an almost spherical photosphere (with deviation of $\lesssim 10\%$) and the spectrum is dominated by hydrogen features. At 31 days the decrease in the strength of the hydrogen lines and the increase in the strength of the helium lines, along with a sharp increase in continuum polarization to $\sim 1\%$, demonstrate that at this epoch the highly asymmetric He core is being revealed. The absorption components of He I 5876Å and 6678Å are observed at 31 days to be highly polarized (to $\sim 0.8\%$). Loops, on the $Q - U$ plane, are observed for H α /He I 6678Å, O I 7774Å and the Ca II IR triplet at 31 days. The presence of these loop features indicates a deviation of the SN ejecta from a global axial symmetry. There is significant rotation of the observed Stokes Q and U parameters, between the first and second epochs, through an angle of $\sim 40^\circ$; indicating that the hydrogen envelope was sufficiently extended to not be coupled to the asymmetries of the He core-layers, associated with the explosion mechanism. The different geometries of the outer envelope layers and the inner core region may be evidence of the “tilted jet” model. SN 2001ig is intrinsically unpolarized at 256 days. The different polarizations at the three epochs show the same physical process observed in Type IIP SNe, of an almost spherically symmetric hydrogen layer shielding a highly asymmetric He core. As time since explosion increases the hydrogen layer becomes optically thin revealing the He core and the polarization is seen to increase. The expansion velocities of the hydrogen and helium in SN 2001ig are significantly higher than observed for 93J-like Type IIb SNe, but are similar to those observed for SN 1987K, and the polarization properties of SN 2001ig show distinct differences from SN 1993J and SN 1996cb, which are mostly due different degrees of line blending. The differences between SN 2001ig and SNe 1993J and 1996cb suggest that Type IIb SNe are not as homogeneous as perhaps previously considered, but may be sufficiently homogeneous to share similar geometries and, potentially, progenitor systems.

Acknowledgements

The authors are grateful to the European Southern Observatory for the generous allocation of observing time. They especially thank the staff of the Paranal Observatory for their competent and never-tiring support of this project in service mode. The research of JRM and JCW is supported in part by NSF grant AST-0406740 and NASA grant NNG04GL00G.

REFERENCES

- Aldering, G., Humphreys, R. M., & Richmond, M. 1994, *AJ*, 107, 662
- Appenzeller, I., Fricke, K., Furtig, W., Gassler, W., Hafner, R., Harkl, R., Hess, H.-J., Hummel, W., & et al. 1998, *The Messenger*, 94, 1
- Blondin, J. M. & Mezzacappa, A. 2007, *Nature*, 445, 58
- Cardelli, J. A., Clayton, G. C., & Mathis, J. S. 1989, *ApJ*, 345, 245
- Clayton, G. C., Wolff, M. J., Gordon, K. D., Smith, P. S., Nordsieck, K. H. & Babler, B. L. 2004, *AJ*, 127, 3382
- Clocchiatti, A. 2002, *IAUC*, 7793, 2
- Cropper, M., Bailey, J., McCowage, J., Cannon, R. D., & Couch, W. J. 1988, *MNRAS*, 231, 695
- Dray, L. M., Dale, J. E., Beer, M. E., Napiwotzki, R., & King, A. R. 2005, *MNRAS*, 364, 59
- Evans, R. O. 2001, *IAUC*, 7772, 1
- Fesen, R. A., & Gunderson, K. S. 1996, *ApJ*, 470, 967
- Filippenko, A. V. 1988, *AJ*, 96, 1941
- Filippenko, A. V. and Matheson, T. and Ho, L. C. 1993, *ApJL*, 415, L103
- Filippenko, A. V., & Chornock, R. 2002, *IAUC*, 7988, 3
- Höflich, P. 1995, *ApJ*, 440, 821
- Höflich, P. 1991, *A&A*, 246, 481

- Höflich, P., Khokhlov, A., & Wang, L. 2001, in American Institute of Physics Conference Series, Vol. 586, 20th Texas Symposium on relativistic astrophysics, ed. J. C. Wheeler & H. Martel, 459
- Howell, D. A., Höflich, P., Wang, L., & Wheeler, J. C. 2001, *ApJ*, 556, 302
- Jeffery, D. J. 1991, *ApJS*, 77, 405
- Jehin, E., O’Brien, K., & Szeifert, T. 2005, FORS1+2 User Manual, 3rd edn., ESO, Garching, VLT-MAN-ESO-13100-1543
- Kasen, D., Nugent, P., Wang, L., Howell, D. A., Wheeler, J. C., Höflich, P., Baade, D., Baron, E., & Hauschildt, P. H. 2003, *ApJ*, 593, 788
- Koribalski, B. S., Staveley-Smith, L., Kilborn, V. A., Ryder, S. D., Kraan-Korteweg, R. C., Ryan-Weber, E. V., Ekers, R. D., Jerjen, H., & et al. 2004, *AJ*, 128, 16
- Kotak, R., & Vink, J. S. 2006, *A&A*, 460, L5
- Leonard, D. C., Filippenko, A. V., Ardila, D. R., & Brotherton, M. S. 2001, *ApJ*, 553, 861
- Leonard, D. C., Filippenko, A. V., Chornock, R., & Foley, R. J. 2002, *PASP*, 114, 1333
- Leonard, D. C., Filippenko, A. V., Chornock, R. & Li, W. 2002, *AJ*, 124, 2506
- Leonard, D. C., Filippenko, A. V., Ganeshalingam, M., Serduke, F. J. D., Li, W., Swift, B. J., Gal-Yam, A., Foley, R. J., Fox, D. B., Park, S., Hoffman, J. L., & Wong, D. S. 2006, *Nature*, 440, 505
- Matheson, T., Filippenko, A. V., Barth, A. J., Ho, L. C., Leonard, D. C., Bershad, M. A., Davis, M., Finley, D. S., Fisher, D., González, R. A., Hawley, S. L., Koo, D. C., Li, W., Lonsdale, C. J., Schlegel, D., Smith, H. E., Spinrad, H., & Wirth, G. D. 2000a, *AJ*, 120, 1487
- Matheson, T., Filippenko, A. V., Ho, L. C., Barth, A. J., & Leonard, D. C. 2000b, *AJ*, 120, 1499
- Maund, J., Wheeler, J., Patat, F., Baade, D., Wang, L., & Höflich, P. 2007, *MNRAS*, in press, astro-ph/0707.2237
- Maund, J. R., Smartt, S. J., Kudritzki, R. P., Podsiadlowski, P., & Gilmore, G. F. 2004, *Nature*, 427, 129

- Mazzali, P. A., Kawabata, K. S., Maeda, K., Nomoto, K., Filippenko, A. V., Ramirez-Ruiz, E., Benetti, S., Pian, E., Deng, J., Tominaga, N., Ohyama, Y., Iye, M., Foley, R. J., Matheson, T., Wang, L., & Gal-Yam, A. 2005, *Science*, 308, 1284
- McCall, M. L. 1984, *MNRAS*, 210, 829
- McCall, M. L., Reid, N., Bessell, M. S., & Wickramasinghe, D. 1984, *MNRAS*, 210, 839
- Phillips, M. M., Suntzeff, N. B., Krisciunas, K., Carlberg, R., Gladders, M., Barrientos, F., Matheson, T., & Jha, S. 2001, *IAUC*, 7772, 2
- Ryder, S., Kranz, K., Sadler, E., & Subrahmanyan, R. 2001, *IAUC*, 7777, 2
- Ryder, S. D., Murrowood, C. E., & Stathakis, R. A. 2006, *MNRAS*, 369, L32
- Ryder, S. D., Sadler, E. M., Subrahmanyan, R., Weiler, K. W., Panagia, N., & Stockdale, C. 2004, *MNRAS*, 349, 1093
- Scarrott, S. M., Ward-Thompson, D., & Warren-Smith, R. F. 1987, *MNRAS*, 224, 299
- Schlegel, D. J., Finkbeiner, D. P., & Davis, M. 1998, *ApJ*, 500, 525
- Serkowski, K., Mathewson, D. L., & Ford, V. L. 1975, *ApJ*, 196, 261
- Shapiro, P. R., & Sutherland, P. G. 1982, *ApJ*, 263, 902
- Soderberg, A. M., Chevalier, R. A., Kulkarni, S. R., & Frail, D. A. 2006, *ApJ*, 651, 1005
- Swartz, D. A., Clocchiatti, A., Benjamin, R., Lester, D. F., & Wheeler, J. C. 1993, *Nature*, 365, 232
- Trammell, S. R., Hines, D. C., & Wheeler, J. C. 1993, *ApJL*, 414, L21
- Tran, H. D., Filippenko, A. V., Schmidt, G. D., Bjorkman, K. S., Jannuzi, B. T., & Smith, P. S. 1997, *PASP*, 109, 489
- Turatto, M., Benetti, S., & Cappellaro, E. 2003, in *From Twilight to Highlight: The Physics of Supernovae*, ed. W. Hillebrandt & B. Leibundgut, 200
- Wang, L., Baade, D., Höflich, P., Khokhlov, A., Wheeler, J. C., Kasen, D., Nugent, P. E., & et al. 2003a, *ApJ*, 591, 1110
- Wang, L., Baade, D., Höflich, P., & Wheeler, J. C. 2002, *The Messenger*, 109, 47
- . 2003b, *ApJ*, 592, 457

- Wang, L., Baade, D., Höflich, P., Wheeler, J. C., Kawabata, K., Khokhlov, A., Nomoto, K., & Patat, F. 2006, ApJ, 653, 490
- Wang, L., Howell, D. A., Höflich, P., & Wheeler, J. C. 2001, ApJ, 550, 1030
- Wang, L., & Wheeler, J. C. 1996, ApJL, 462, L27
- Wang, L., Wheeler, J. C., & Höflich, P. 1997, ApJL, 476, L27
- Wang, L., Wheeler, J. C., Höflich, P., Khokhlov, A., Baade, D., Branch, D., Challis, P., et al. 2002, ApJ, 579, 671
- Wheeler, J. C., & Akiyama, S. 2007, ApJ, 654, 429
- Wheeler, J. C, Maund, J. R. & Couch, S. M. 2007, ApJ, Submitted
- Woosley, S. E., & Bloom, J. S. 2006, ARAA, 44, 507

Table 1: Journal of Spectropolarimetric Observations of SN 2001ig

Star	Date	Exposure (s)	Wavelength (Å)	Air Mass	Filter	Comment
SN 2001ig	2001 Dec 16.11	4×1000	4450-8635	1.86	GG435	SN
HD 49798	2001 Dec 16.12	10	4450-8635	1.31	GG435	Flux STD
LTT 9491	2002 Jan 03.02	200	4450-8635	1.47	GG435	Flux STD
SN 2001ig	2002 Jan 03.07	4×500	4450-8635	2.19	GG435	SN
EG 274	2002 Aug 15.98	60	3700-8635	1.03	None	Flux STD
SN 2001ig	2002 Aug 16.26	4×1200	3700-8635	1.04	None	SN
GD 50	2002 Aug 16.44	60	3700-8635	1.09	None	Flux STD

All observations conducted with the GRIS-300V grism.

Table 2: Prominent P Cygni Profiles and Velocities at Absorption Minimum at +13 and +31 days

Line	Epoch	
	+13 days	+31 days
	v (km s ⁻¹)	v (km s ⁻¹)
Fe II 5169Å	blended	-10 300
He I 5876Å	-14 000	-12 000
Si II 6355Å	...	-8 000
H α	-19 000	-13 600
He I 6678Å	-19 000	-12 000
O I 7774Å	-12 700	-10 600
Ca II IR triplet	-12 700	-12 400

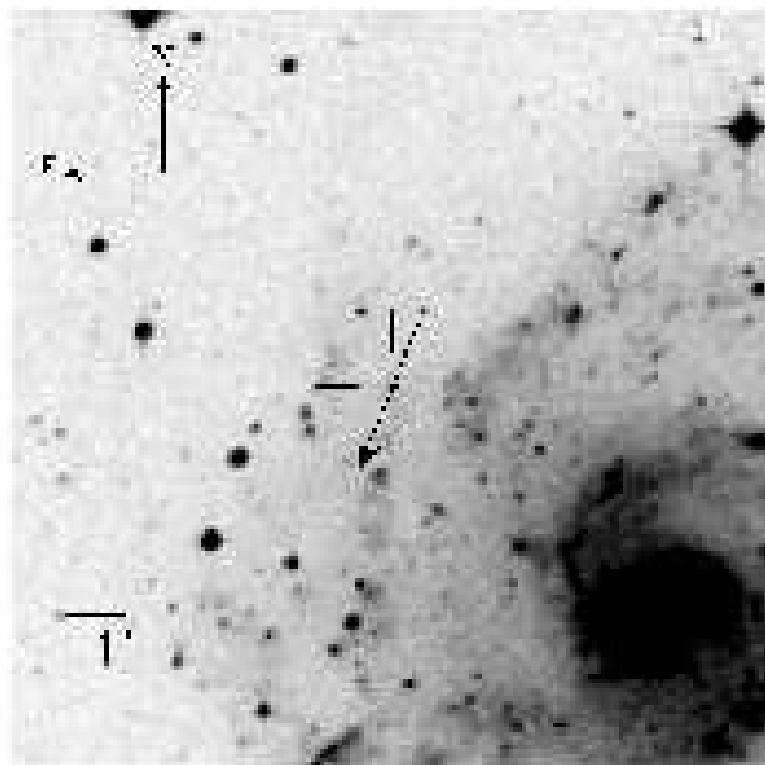


Fig. 1.— Digital Sky Survey image of the location of SN 2001ig, shown by the filled black circle and cross hairs, relative to its host galaxy NGC 7424. The arrow shows the orientation of the Interstellar Polarization component determined in Section 3.2.3.

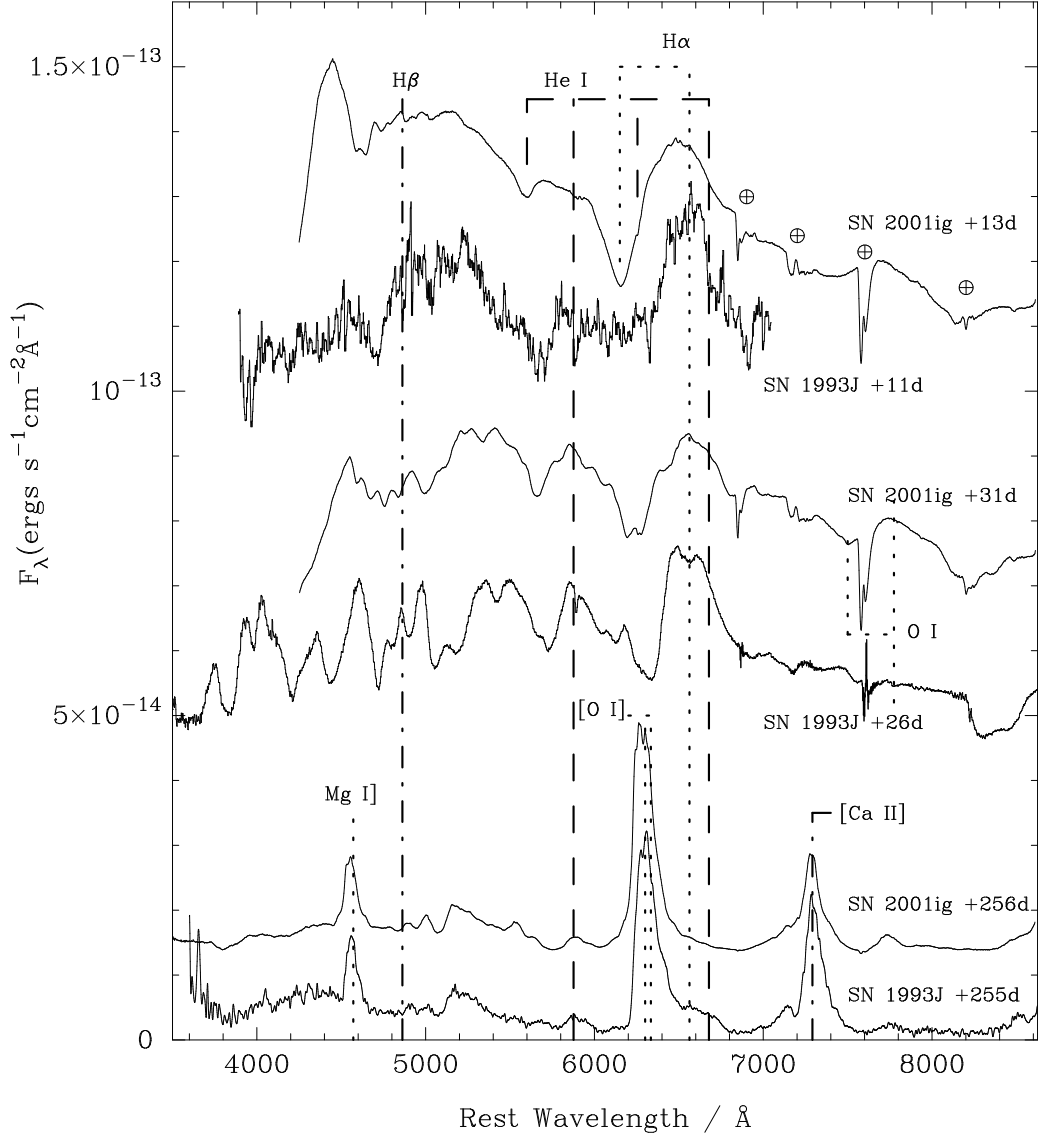


Fig. 2.— Flux spectra of SN 2001ig at 2001 Dec 16, 2002 Jan 3 and 2002 Aug 16 (or 13, 31 and 256 days post-explosion respectively). Line identifications follow Matheson et al. (2000a). Telluric lines are indicated by the \oplus symbol. Also shown are spectra of SN 1993J, from the SUSPECT archive, similarly scaled for similar post-explosion epochs, as given on the figure, using the explosion date of SN 1993J of Tran et al. (1997). The vertical lines show the rest wavelengths and, where appropriate, the associated absorption profile. The wavelengths of these spectra have been corrected for the recessional velocities of the host galaxies of these two SNe.

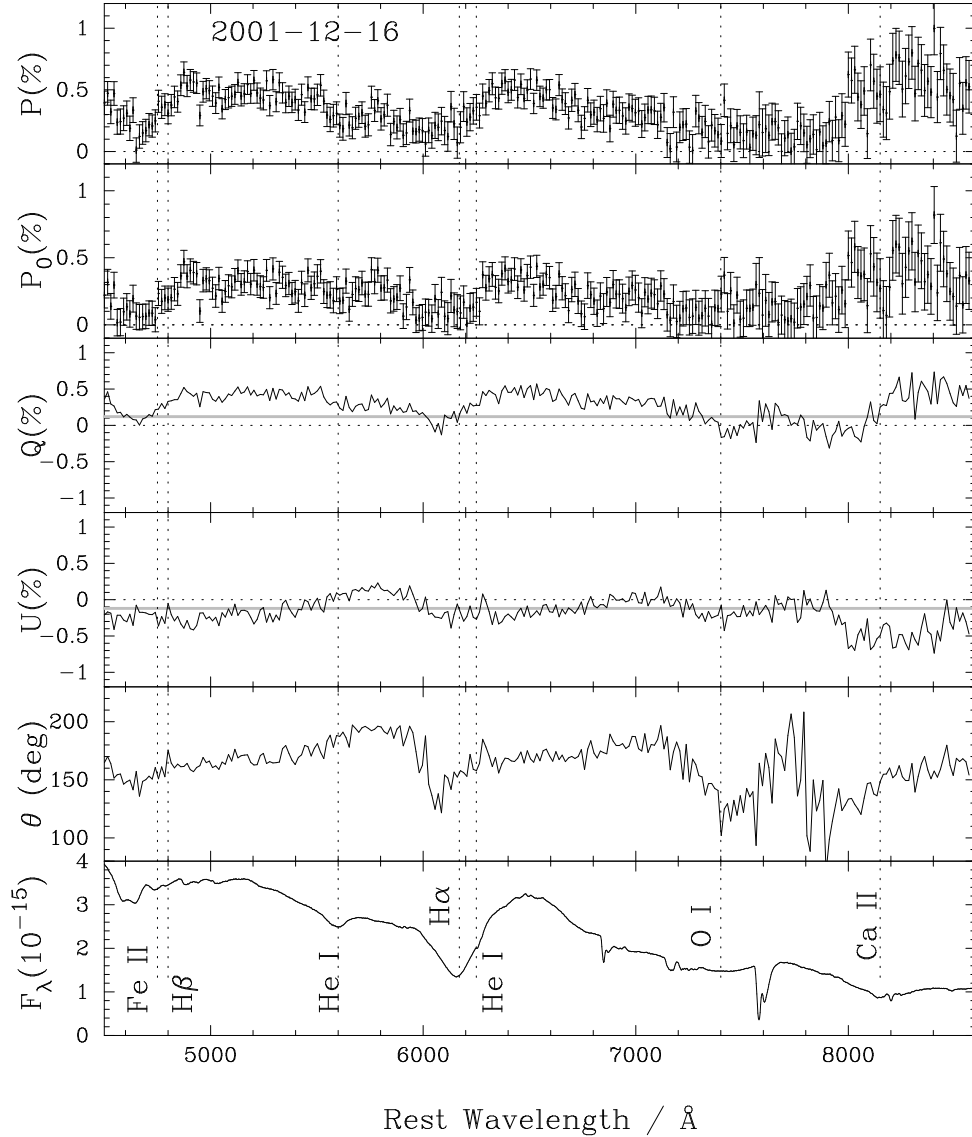


Fig. 3.— Spectropolarimetry of SN 2001ig, acquired on 2001 Dec 16 (13 days post-explosion), showing the total observed polarization p , the total polarization after correction for the ISP p_0 , the Stokes Q and U parameters, the polarization angle θ and the total flux spectrum ($\text{ergs s}^{-1} \text{cm}^{-2} \text{\AA}^{-1}$). The Stokes parameters have been re-binned to 15\AA . The thick grey lines indicate the position of the ISP Stokes Q and U parameters, effectively the zero-point for the Stokes parameters intrinsic the SN. The zeropoint for observed Q and U is indicated by the horizontal dotted line. All data is presented with the wavelength scale corrected for the heliocentric recessional velocity of the host galaxy.

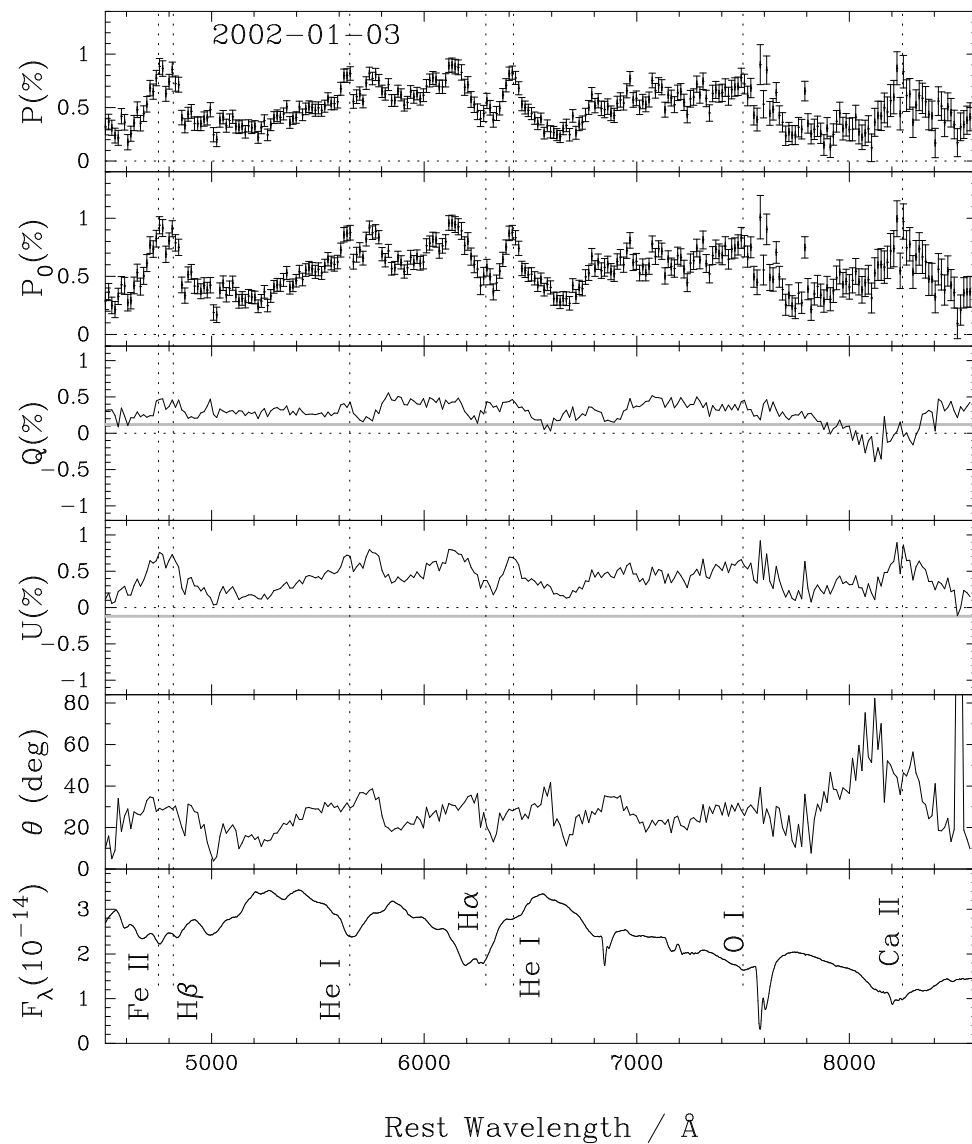


Fig. 4.— Same as Fig. 3, but for spectropolarimetry of SN 2001ig acquired on 2002 Jan 3 (31 days post-explosion). The data is uncorrected for the ISP. Note the small dispersion of the polarization angle θ , compared to the earlier epoch of Fig. 3.

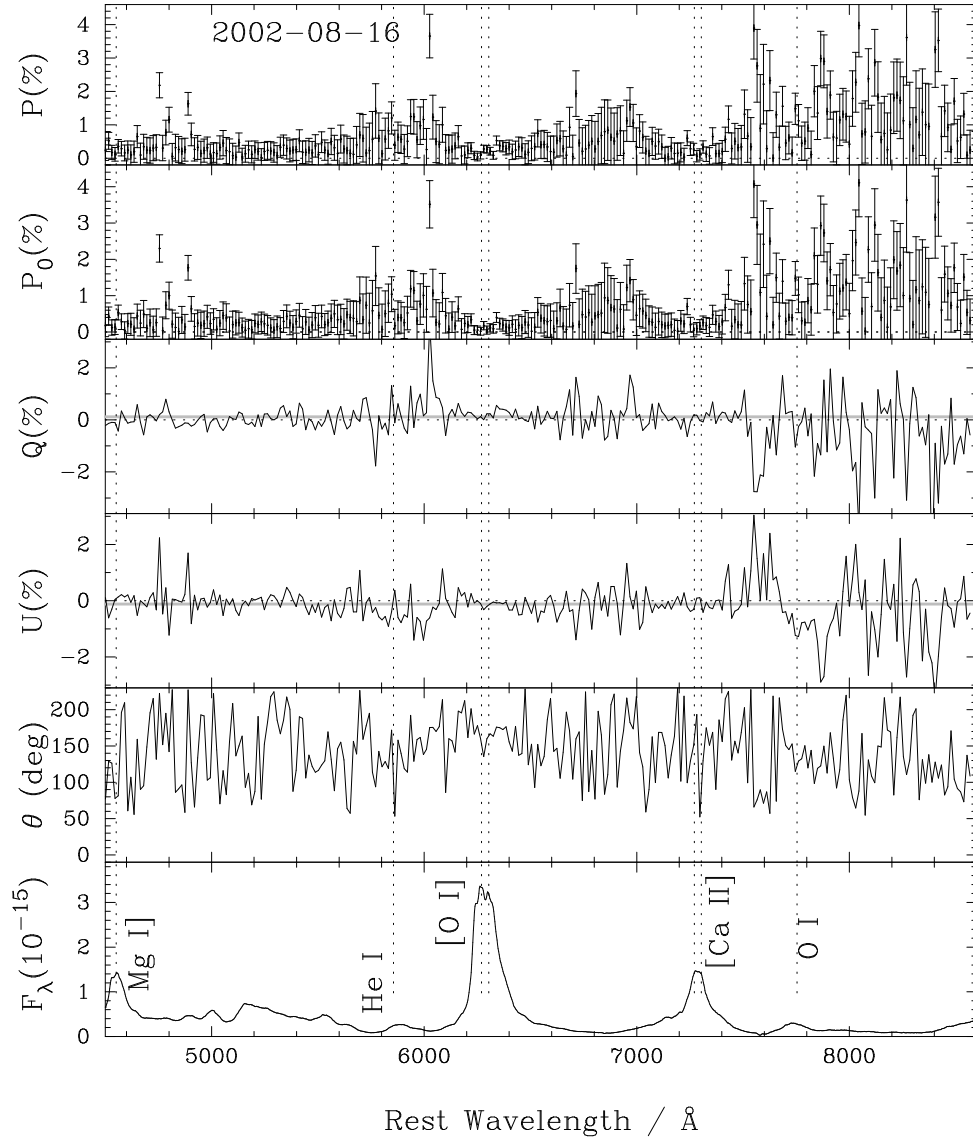


Fig. 5.— Same as Fig. 3, but for spectropolarimetry of SN 2001ig acquired on 2002 Aug 16 (256 days post-explosion).

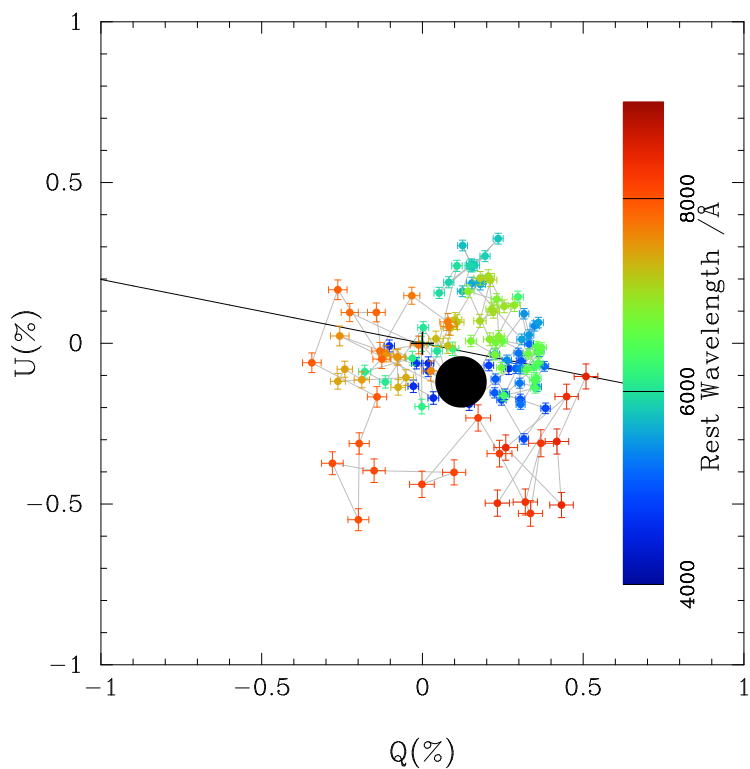


Fig. 6.— Stokes Q and U parameters, as a function of wavelength from observations acquired on 2001 Dec 16 (13 days post-explosion). The Stokes parameters have been re-binned to 50\AA . The data have been corrected for the ISP (shown as the solid black circle; see text). The dominant axis (see text) is indicated by the straight line. The wavelength of each point is indicated by the colour, following the scheme of the colour bar on the right hand side. The location of the origin of the Stokes plane ($Q = 0$ and $U = 0$) is indicated by cross.

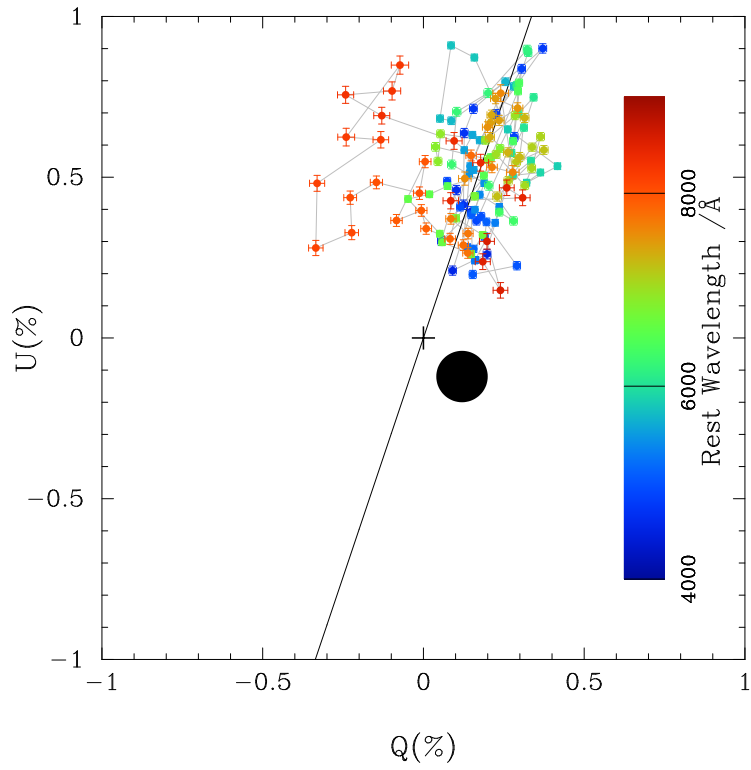


Fig. 7.— Same as Fig. 6, but for spectropolarimetry of SN 2001ig acquired on 2002 Jan 3 (31 days post-explosion). Note that the dominant axis has rotated *physically* $\sim 40^\circ$ compared to that of the earlier epoch of Fig. 6.

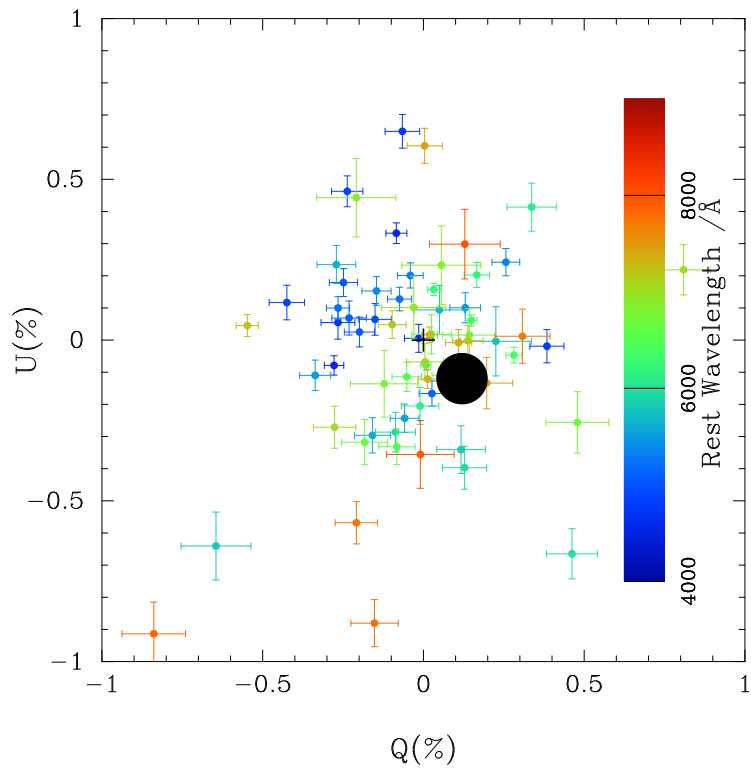


Fig. 8.— Same as Fig. 6, but for spectropolarimetry of SN 2001ig acquired on 2002 Aug 16 (256 days post-explosion).

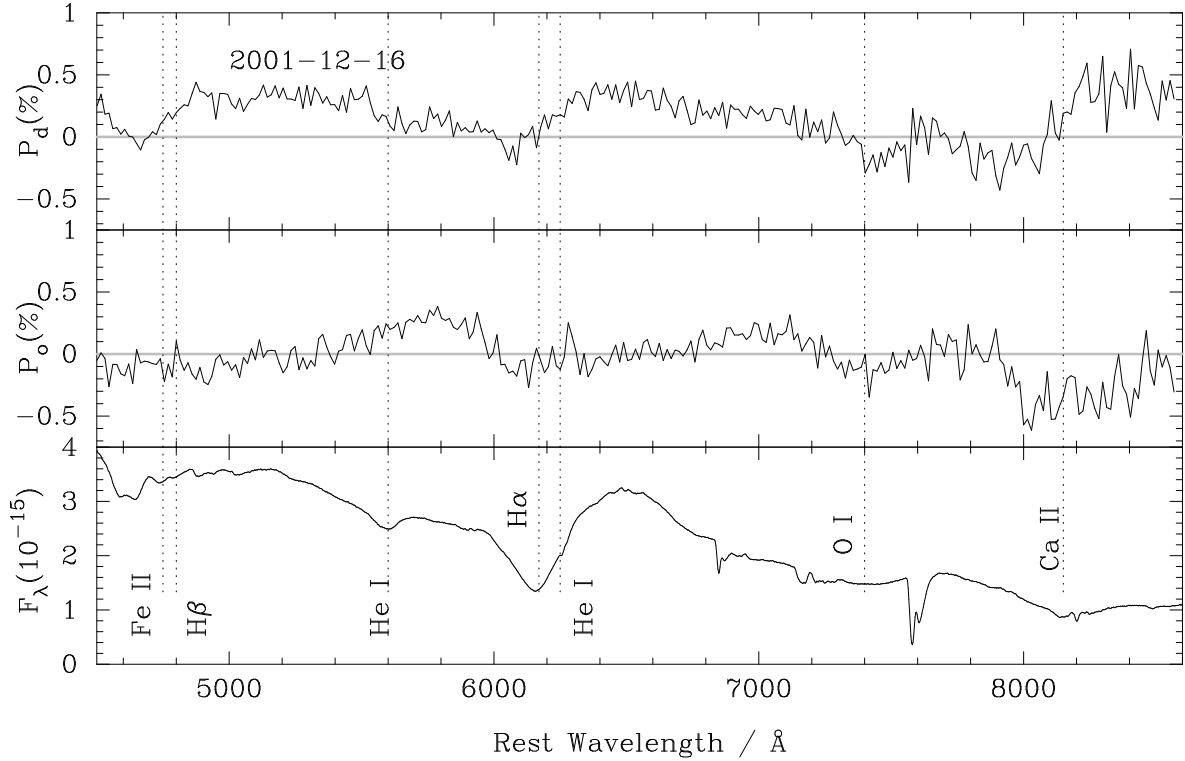


Fig. 9.— The Stokes parameters, corrected for the ISP, rotated to the dominant (P_d) and orthogonal axes (P_o) for the data of 2001 Dec 16, compared with the flux spectrum at this epoch. There is little difference between these rotated Stokes parameters and the Q and U Stokes parameters (Fig. 3), since the dominant axis is nearly aligned ($\theta_d = 4.5^\circ$) with the Q axis. Zero polarization is indicated by the heavy grey line.

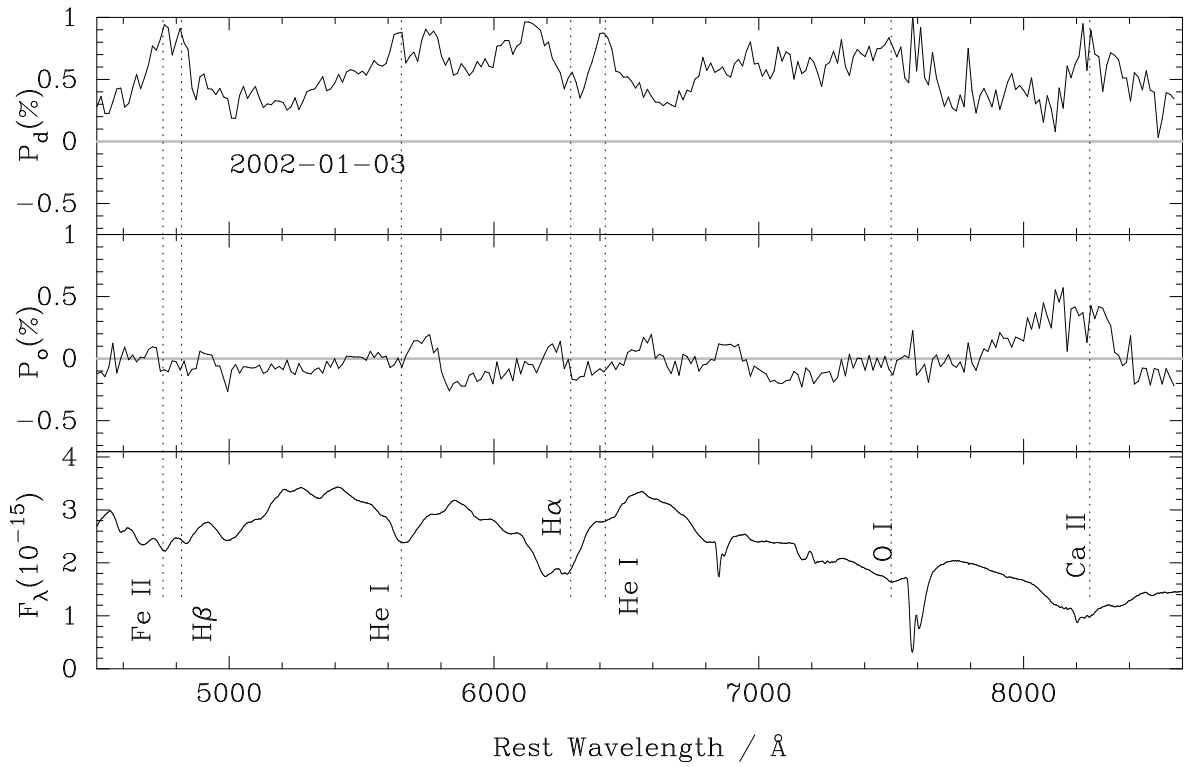


Fig. 10.— The Stokes parameters, corrected for the ISP, rotated to the dominant (P_d) and orthogonal axes (P_o) for the data of 2002 Jan 03, compared with the flux spectrum at this epoch. Zero polarization is indicated by the heavy grey line.

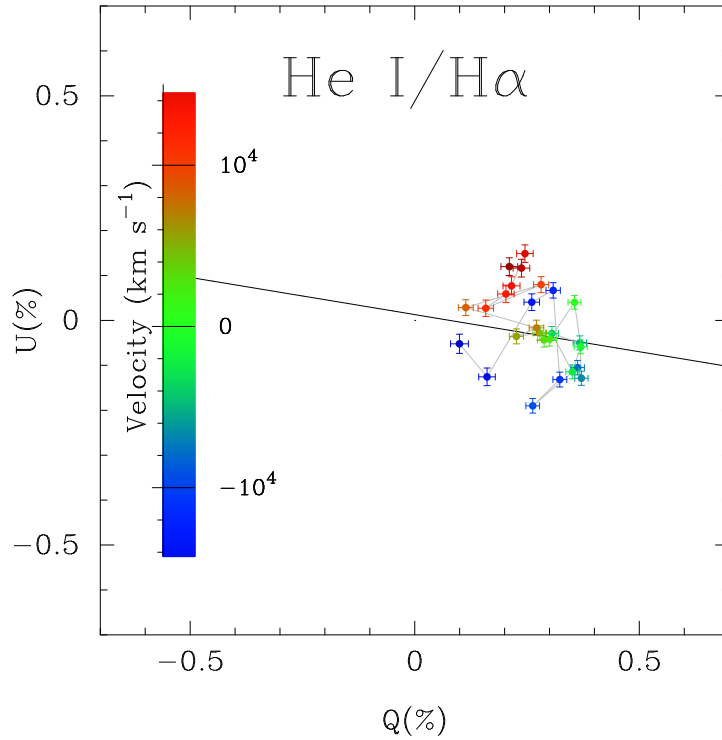


Fig. 11a.— Loops on the Q-U plane for H α /He I 6678 \AA blend, the wavelength range covering O I 7774 \AA , Fe II lines in the range 4800-5600 \AA , and Ca II IR absorption from the observations of 2001 Dec 16. The data have been re-binned to 15 \AA . The heavy dashed line indicates the dominant axis, calculated for the entire data set for this epoch shown as shown on Fig. 6.

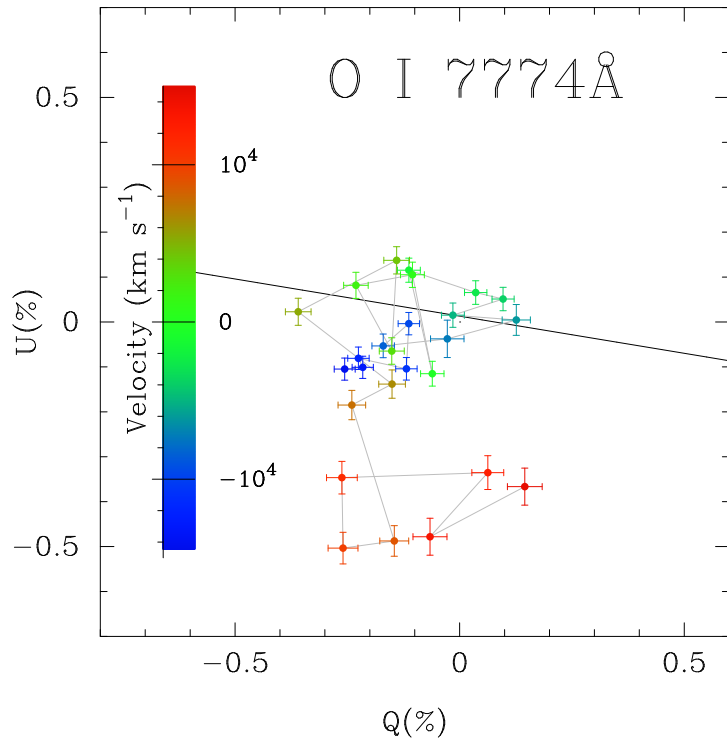


Fig. 11b.—

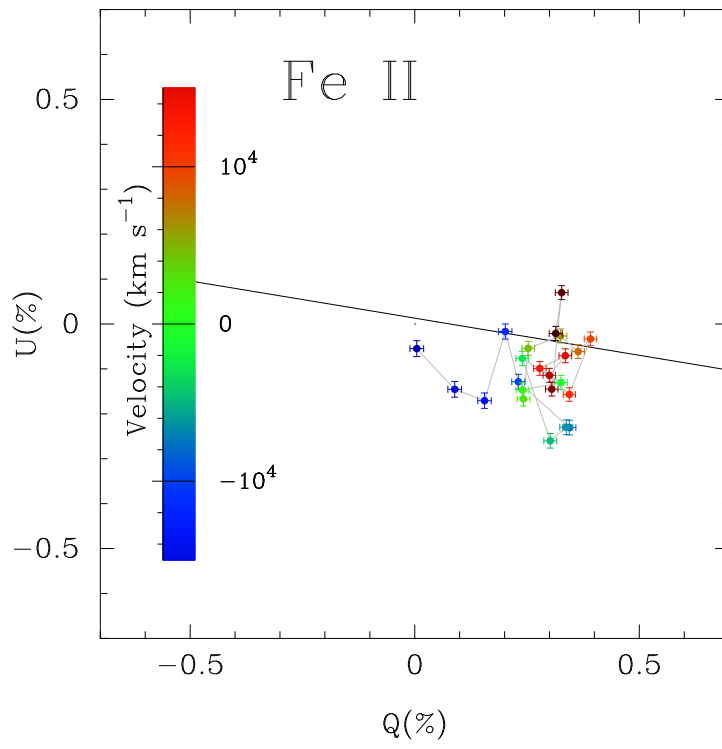


Fig. 11c.—

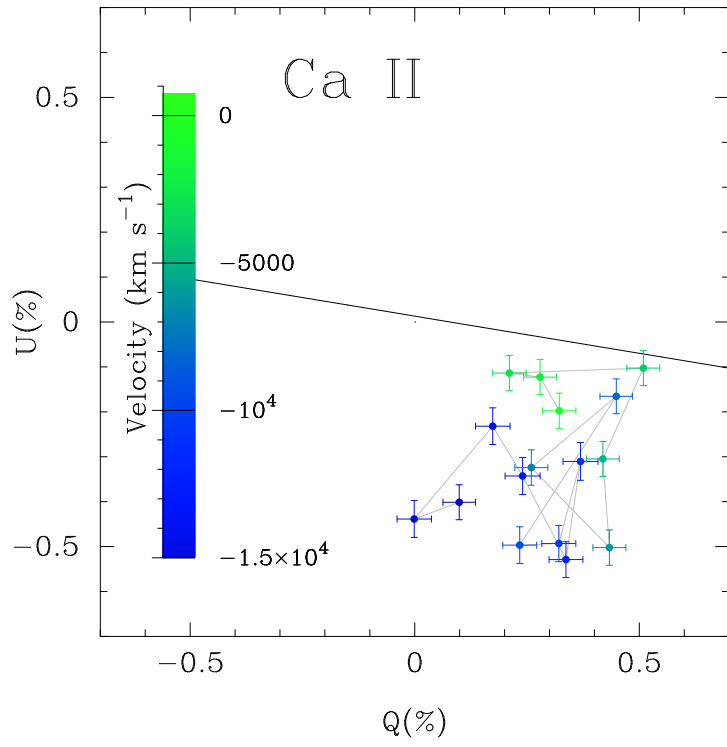


Fig. 11d.—

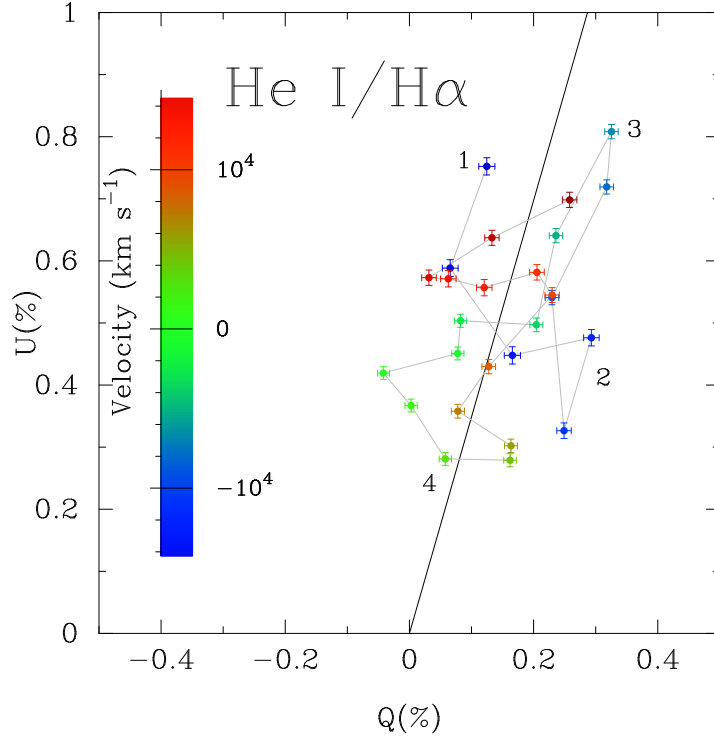


Fig. 12a.— Loops on the Q-U plane for a) $H\alpha$ /He I 6678Å blend (Points of interest are indicated by the numbers, following the wavelength progression of the data on the Stokes plane: 1) Blue edge of the $H\alpha$ absorption profile in the flux spectrum; 2) Absorption minimum of $H\alpha$, 3) Absorption minimum of He I 6678Å; and 4) The $H\alpha$ and He I 6678Å depolarizing emission feature), b) O I 7774Å, c) Fe II lines in the range 4800-5600Å, and d) Ca II IR absorption from the observations of 2002 Jan 3. The data have been re-binned to 15Å. The heavy dashed line indicates the dominant axis, calculated for the entire data set for this epoch shown as shown on Fig. 7. For Ca II the dominant axis determined at the first epoch is shown as the dot-dashed line.

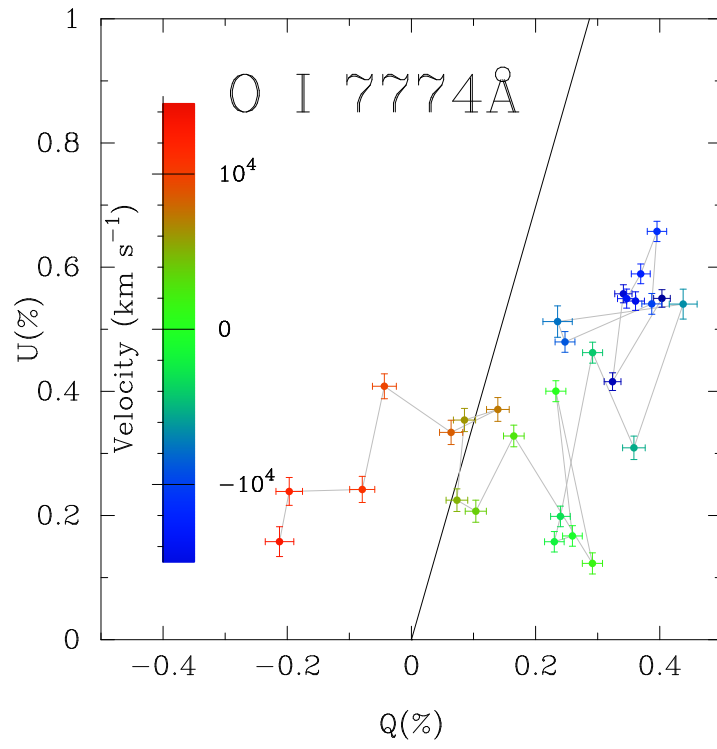


Fig. 12b.—

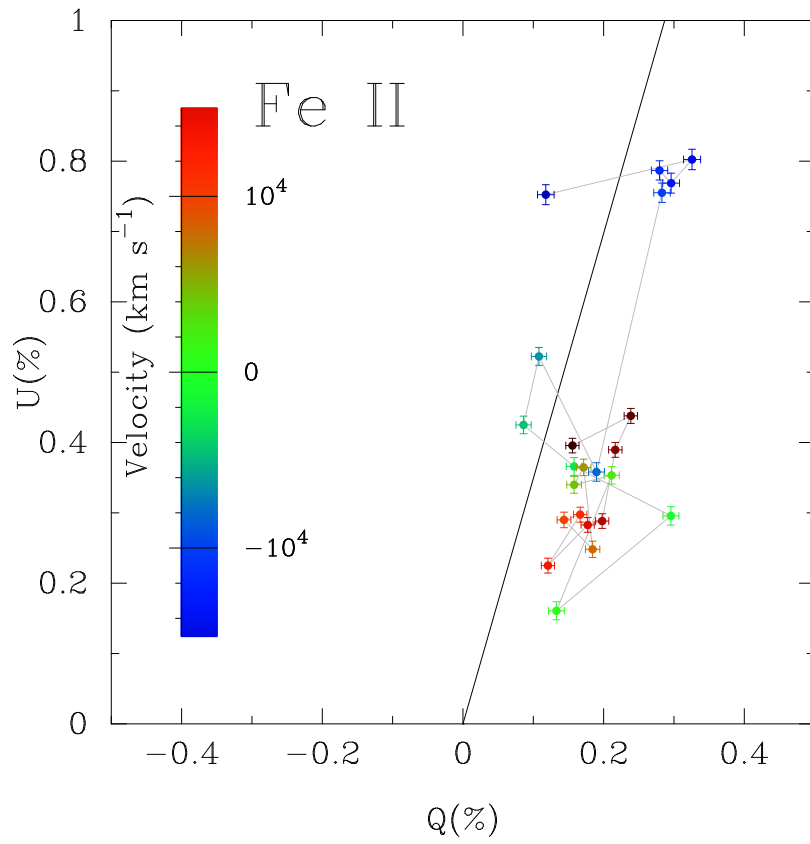


Fig. 12c.—

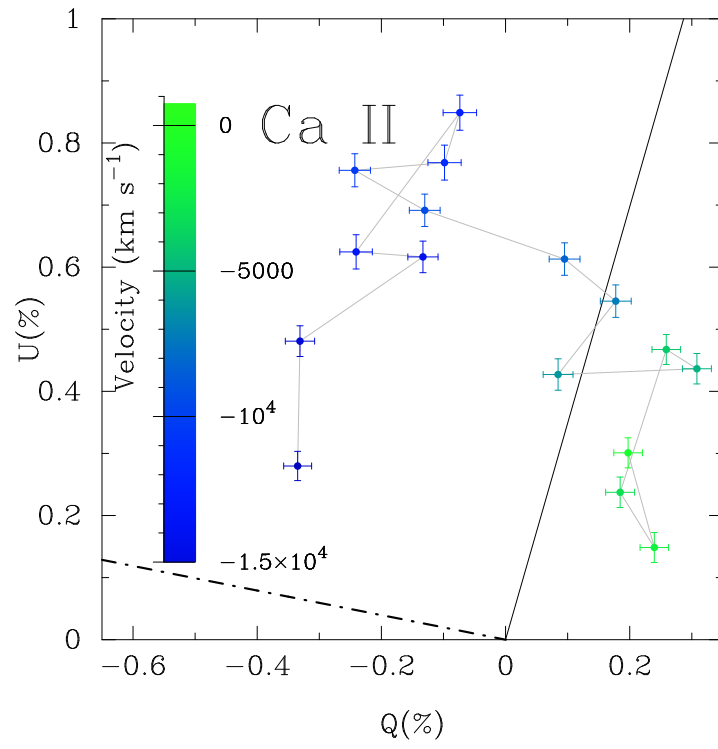


Fig. 12d.—